

MASTER

Nullspace-Based Fault Diagnosis for High-Precision Mechatronics

Munns, Paul

Award date:
2023

[Link to publication](#)

Disclaimer

This document contains a student thesis (bachelor's or master's), as authored by a student at Eindhoven University of Technology. Student theses are made available in the TU/e repository upon obtaining the required degree. The grade received is not published on the document as presented in the repository. The required complexity or quality of research of student theses may vary by program, and the required minimum study period may vary in duration.

General rights

Copyright and moral rights for the publications made accessible in the public portal are retained by the authors and/or other copyright owners and it is a condition of accessing publications that users recognise and abide by the legal requirements associated with these rights.

- Users may download and print one copy of any publication from the public portal for the purpose of private study or research.
- You may not further distribute the material or use it for any profit-making activity or commercial gain

Nullspace-Based Fault Diagnosis for High-Precision Mechatronics

Master Thesis

Paul Munns (1522795)

Supervisor:
prof.dr.ir. Tom Oomen

Advisor:
ir. Koen Classens

Eindhoven, January 2023

*This report was made in accordance with the TU/e Code of Scientific Conduct for
the Master thesis*

Graduation committee:

Chair: prof.dr.ir. Tom Oomen
Members: prof.dr.ir. W.P.M.H. (Maurice) Heemels
 prof.dr.ir. Carlos Murguia
Advisor: ir. Koen Classens

Abstract

To reduce unscheduled production downtime in high-precision mechatronics it is key to detect faults early within the system. To this end, fault diagnosis systems are crucial, and a design strategy, specifically tailored to high-precision systems, is presented to detect and localize actuator and sensor faults. The employed fault diagnosis system builds upon a state-of-the-art nullspace based paradigm and is validated via experiments on a flexible beam set-up and a high-precision next generation wafer stage.

Preface

I'm extremely grateful to my supervisor Koen Classens for his guidance and feedback. The many in-depth discussions and conversations helped me to further develop my analytical skills. I would like to extend my sincere thanks to Prof. Tom Oomen and Jeroen van de Wijdeven from ASML for inspiring me to find new research subjects and case-studies. Next, I would like to thank Eindhoven university of technology and ASML, for providing the experimental facilities. In addition, I am gratefully thankful for the help of my fellow student Mike Mostard for his help providing models and MATLAB scripts for the experimental setups. Lastly, special thanks to my family, fellow students, friends and girlfriend for supporting me through this academic year.

Contents

1	Introduction	1
2	Problem formulation	2
3	Nullspace-based fault diagnosis	5
3.1	Fault detection setting	5
3.2	Exact fault detection problem	6
3.2.1	Nullspace method	6
3.2.2	Achieving least order detector(s)	9
3.2.3	Enforcing stability and desired dynamics	9
3.3	Approximate fault detection problem	11
3.3.1	Attenuation of noise	11
3.4	Fault detection and isolation problem	12
4	Design freedom and limitation	13
4.1	Design freedom	13
4.1.1	Disturbances characterization in motion systems	13
4.1.2	Nullspace computations	13
4.1.3	Noise characterization in motion systems	13
4.1.4	Pole instability threshold <i>smarg</i>	13
4.1.5	Pole relocation <i>sdeg</i>	14
4.1.6	Minimality	14
4.2	Limitation on fault isolation	14
4.3	Overview	16
5	Towards fault diagnosis oriented models	18
5.1	Models in high-precision systems	18
5.2	Models for fault diagnosis	18
5.2.1	Plant model	19
5.2.2	Disturbance model	19
5.2.3	Noise model	20
5.2.4	Fault model	20
6	Application to high-tech precision systems	21
6.1	Detecting actuator and sensors faults for suspended systems	21
6.1.1	Experimental beam setup	21
6.1.2	FDI design beam setup	22
6.1.3	Result	23
6.2	Detecting actuator and sensors faults for unsuspended systems	24
6.2.1	Experimental setup	24
6.2.2	FDI design	26
6.2.3	Result	27
6.3	Real-time interference decoupling	28
6.3.1	Cable slab behaviour	28
6.3.2	FDI design for cable slab detection	29
6.3.3	Result	29

7	Conclusions & Recommendations	31
7.1	Conclusions	31
7.2	Recommendations	31
	Appendix	33
A	Example of the loss of strong fault detectability for sensor faults in unsuspended systems	34
B	Example of limitation of fault isolation in high-tech precision systems	35
C	Example of losing strong fault detection when employing minimality	37
D	Closed-loop transfer functions for nullspace-based fault diagnosis	38
E	Example loss of fault isolability due to row and column independency	40

Chapter 1

Introduction

Fault diagnosis is becoming increasingly important in the field of process monitoring due to the growing demand of systems that require higher performance, safety and reliability [1]. This requires the fault diagnostic systems to execute its functionalities under more complex operation conditions, which include the identification of faults in machines, the localization of faults in machines, and the prediction of the remaining life-time of components. Fault diagnostic systems are therefore one of the key techniques for predictive maintenance. Predictive maintenance allows for efficient planning of the maintenance operation of the machine tools and reduces the unscheduled production downtime, which is essential in high-tech precision systems [2].

For decades, research in the field of fault diagnosis has been devoted to model-based fault diagnosis and data-driven fault diagnosis. Currently, due to advancements in the field of artificial intelligence, a significant part of research is focused on data-driven fault diagnosis [3]–[5]. However, the downside of these data-driven methods is that the quality of the algorithm is dependent on the quality and quantity of the training data, which is not always available [6].

In contrary to the data-driven approach for fault diagnosis, a model-based approach requires only the availability of the system model. Additionally, the model-based approach gives more insight into the fault diagnostic system. Numerous model-based approach for fault diagnosis and their computations have been described in [7], however, the recently developed nullspace-based fault diagnosis in [8], is the first model-based approach that provides a complete collection of numerically reliable methods for the synthesis of a fault diagnostic system for large-scale systems.

While the application of the nullspace-based fault diagnosis has been extensively studied in the aerospace industry [8]–[10], the application to the field of high-tech precision systems is still limited. These are often multi-input multi-output (MIMO) interconnected systems, in which accuracy performance is key. Such systems can be represented via linear models, which are possibly of high order due to flexible dynamics in case of high performance and high degrees of freedom (DOF) [11]. Hence, the possibility and limitation of the nullspace-based fault diagnosis on these systems is currently unknown.

Additionally, the model-based fault diagnosis approach requires an accurate model of the system plant G . Currently, the models that are obtained in high-tech precision systems, are derived for modelling and control purposes. However, it is unclear what the requirements for fault diagnosis oriented models are. In particular, in what frequency range is model accuracy required.

Furthermore, with the presence of interconnected submodules in a high-precision system, the complexity and scale of fault diagnostic systems is increased. Therefore, it is desirable to employ fault diagnosis on submodule level, to simply the fault localization problem, i.e., to enable to pinpoint the faulty submodule without modelling the entire system. This introduces new challenges to the fault diagnostic system.

The outline of this thesis is as follows; Chapter 2 describes the problem formulation. The theory of the nullspace-based fault diagnosis is described in Chapter 3. Chapter 4 describes the design freedom and limitations of the nullspace-based approach on high-precision systems. The model requirements for effective model-based fault diagnosis are given in Chapter 5. Chapter 6 investigates two case-studies. In the first case-study, the nullspace-based fault diagnosis is employed to detect and locate multiple actuator and sensor faults injected into high-precision systems. In the second case-study, the nullspace-based fault diagnosis is employed to cope with interference between submodules in high-precision systems. Finally, a conclusion and recommendation is given in Chapter 7.

Chapter 2

Problem formulation

Consider the nullspace-based fault diagnosis for a closed-loop MIMO system, as depicted in Fig 2.1. The residual generator Q processes the known control inputs u and the available measurements y to generate a residual signal ε . The residual signal indicates the presence or absence of a fault f and is insensitive to the reference signal r , disturbance signal d and noise signal w . The synthesis of Q is based on the model of system G , which is composed of the model of the plant G_u , the disturbance G_d , the noise G_w and the fault G_f . In MIMO systems, the model G_u consists of large-scale models with complex interconnections.

Remark. *The nullspace-based fault diagnosis, mainly focusses on additive faults, such as actuator and sensor faults.*

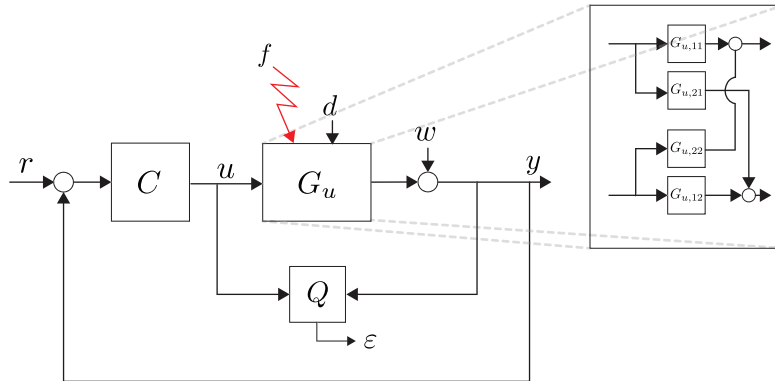


Fig. 2.1: The configuration of the nullspace-based fault diagnosis in a closed-loop MIMO system, where G_u contains numerous interaction terms. The filter Q processes the control input u and measurement y , and outputs the residual ε that indicates whether fault f is present or absent.

The intention of this report is to investigate the use of nullspace-based fault diagnosis for high-tech precision systems. Since, the nullspace-based approach for fault diagnosis is primarily developed for the aerospace industry, the possibility and limitation of the nullspace-based approach within high-precision systems need to be defined. Furthermore, the nullspace-based approach requires an accurate model representation of the system. However, a quantification of this accuracy is required for effective fault diagnosis. Lastly, validation of this approach is required to demonstrate its applicability within the industry. Hence, the following three research questions are posed:

1. What is the design freedom and limitation of nullspace-based fault diagnosis tailored to high-tech precision systems?
2. Where is model accuracy required for the synthesis of effective fault detection filters? In other words, in what frequency range should modelling errors be avoided?
3. Application of nullspace-based fault diagnosis on full MIMO high-tech positioning systems.
 - (a) Detection and localization of actuator and sensor faults on a full MIMO application, e.g., the flexible beam and overactuated test rig (OAT).
 - (b) Interference decoupling on a full MIMO application for submodule level fault diagnosis. This is demonstrated on the OAT.

The answers to these questions form important insights, crucial for fault diagnosis system design for high-tech positioning systems.

Research question (1):

The nullspace-based fault diagnosis synthesis, described in [8], contains a vast amount of synthesis options. Numerous design examples are demonstrated on systems originating from the aerospace industry. However, high-tech precision systems differ from aerospace systems in scale and complexity. Hence, the design freedom and limitations of the synthesis should be investigated for high-tech systems.

Research question (2):

Ideally, a model should be an accurate representation of the true system over the entire frequency range. However, in practice, the model is an approximation of the real system. Hence, it can only give a good approximation over a certain range of frequencies. Models used for control purposes, usually demands high accuracy around the flexible modes to guarantee high performance. These models are generally obtained via identification techniques, which are able to obtain the model in an inexpensive, fast and accurate approach [12]. However, it is unclear whether these identified models designed for control purposes are also suited for fault diagnosis. This might require a different approach to the system identification procedure. Hence, a clear requirement for model accuracy for model-based fault diagnosis should be developed. Primarily focusing on model accuracy in certain frequency ranges.

Research question (3):

The applicability of the nullspace-based approach for fault diagnosis on high-precision systems, is demonstrated on two common types; suspended and unsuspended. The two experimental setups that are used for demonstration purposes are; the flexible beam (suspended) and the OAT (unsuspended), depicted in Fig. 2.2(a) and Fig. 2.2(b), respectively. Both systems have different

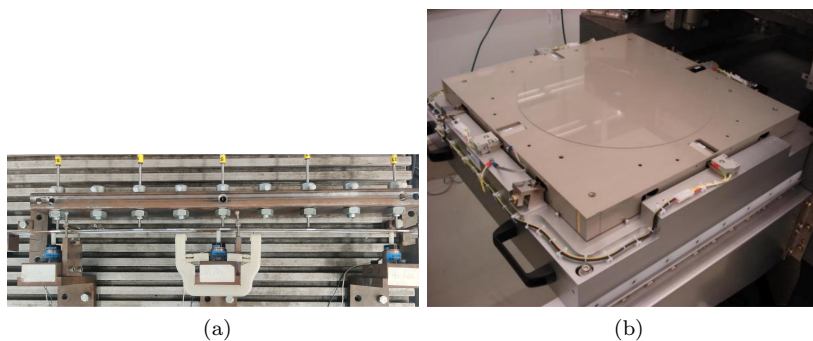


Fig. 2.2: The flexible beam setup (a) and the overactuated test rig (OAT) (b).

rigid-body dynamics, which affects the possibility and limitation of the nullspace-based fault diagnosis. A suspended system is connected to the fixed-world, e.g., via a spring, and their bode diagrams starts with a '0'-slope. An unsuspended system levitates, which leads to poles present at the origin. Hence, their bode diagrams starts with a '-2'-slope. Both experimental setups are MIMO systems having a vast amount of actuators and sensors. Hence, to detect and localize faults in these actuators and sensors, a nullspace-based fault diagnosis system is required.

Additionally, the OAT can be used to demonstrate the interference decoupling for submodule level fault diagnosis. The necessity for this submodule fault diagnosis derives from the state-of-the-art high-precision system, e.g., lithography systems, which are often composed of multiple inter-connecting submodules, e.g., the TWINSCAN NXT1950i from ASML, depicted in Fig 2.3. The machine consists of a long stroke short stroke actuation platform to achieve nanometer positioning performance with high throughput.

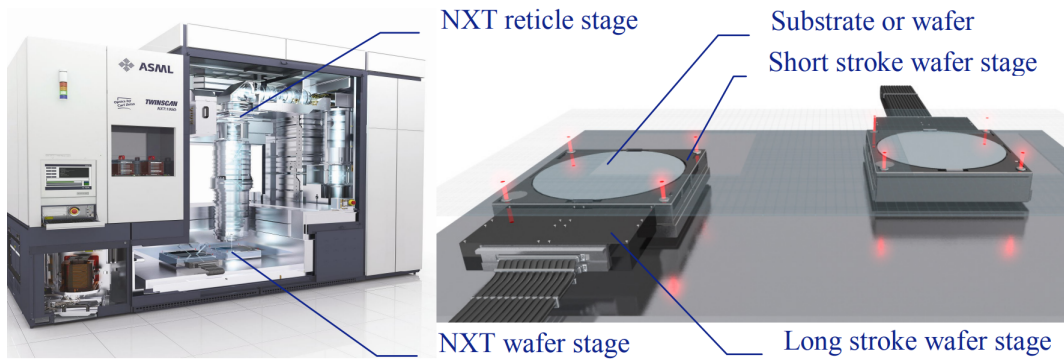


Fig. 2.3: The TWINSCAN NXT1950i from ASML with the dual substrate stage [13]. The stage contains long stroke and short stroke actuators which are connected to the fixed world via a cable slab.

To power the electromotors in the fast-moving wafer stage, a cable slab is used, which connects the wafer stage to the rest of the machine. This introduces disturbances via the cable slab, which can lead to interference in the fault diagnosis system. Therefore, it is highly important to include the interference introduced by the cable slab during the synthesis of the fault diagnosis system for the wafer stage (submodule level). This requires a new adaptation for the nullspace-based fault diagnosis approach to cope with this cable slab interference d_{cable} , depicted in Fig 2.4.

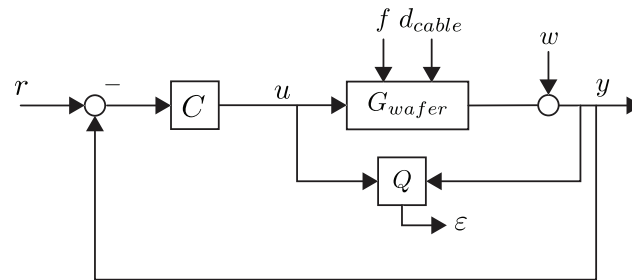


Fig. 2.4: A closed-loop configuration of a wafer stage, including the interferences from the cable slab d_{cable} . The fault detection filter Q output the residual ϵ , that detects faults f while the disturbance from d_{cable} is present.

Chapter 3

Nullspace-based fault diagnosis

In this chapter the nullspace-based fault diagnosis synthesis is described. The chapter starts with the general fault detection setting. Next, solving the exact fault detection problem is explained and is further expanded to the approximate fault detection problem which copes with sensor noise. Eventually, the problem is extended to an isolation problem to localize faults.

3.1 Fault detection setting

Consider the system presentation in Fig 3.1. The representation is in λ since it can be both presented in continuous and in discrete time, i.e. $\lambda = s$ and $\lambda = z$ respectively. The fault detector filter, highlighted in (■), is defined as $Q(\lambda) := [Q_y(\lambda) \ Q_u(\lambda)]$ and processes the sensor signal $y(\lambda)$ and the control input signal $u(\lambda)$, and outputs the residual signal $\varepsilon(\lambda)$.

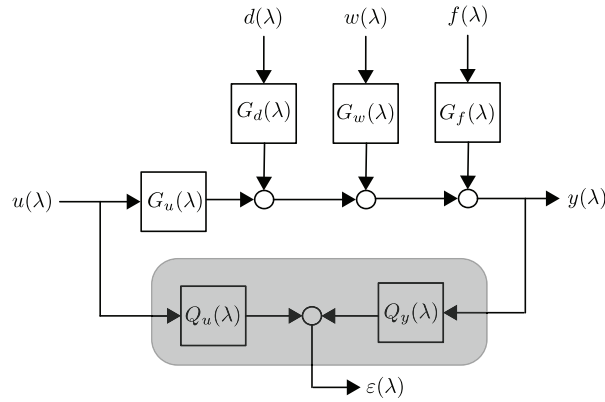


Fig. 3.1: Standard open-loop configuration of a fault diagnosis system. The fault detection filter $Q(\lambda)$ is highlighted in (■), which outputs the residual signal $\varepsilon(\lambda)$ that indicates whether fault $f(\lambda)$ is present or absent.

The output signal $y(\lambda)$ can be formulated as

$$y(\lambda) = G_u(\lambda)u(\lambda) + G_d(\lambda)d(\lambda) + G_w(\lambda)w(\lambda) + G_f(\lambda)f(\lambda), \quad (3.1)$$

where $y(\lambda)$ is a p -dimensional vector, control input $u(\lambda)$ is a m_u -dimensional vector, $d(\lambda)$ is m_d -dimensional vector, $w(\lambda)$ is a m_w -dimensional vector and $f(\lambda)$ is a m_f -dimensional vector. There are no required criteria for the transfer function matrices (TFMs) $[G_u(\lambda) \ G_d(\lambda) \ G_f(\lambda) \ G_w(\lambda)]$, e.g., (strictly) properness or stability. The residual $\varepsilon(\lambda)$ can be described via the following form

$$\varepsilon(\lambda) = Q(\lambda) \begin{bmatrix} y(\lambda) \\ u(\lambda) \end{bmatrix} = Q_y(\lambda)y(\lambda) + Q_u(\lambda)u(\lambda). \quad (3.2)$$

An important condition is that $Q_y(\lambda)$ and $Q_u(\lambda)$ are proper and stable. Loosely speaking, the objective of fault detector filter $Q(\lambda)$ is to output a residual $\varepsilon(\lambda)$ such that

$$\begin{aligned}\varepsilon(\lambda) &\approx 0, \text{ when } f(\lambda) = 0, \\ \varepsilon(\lambda) &\neq 0, \text{ when } f(\lambda) \neq 0,\end{aligned}\tag{3.3}$$

for all disturbance input $d(\lambda)$ and control input $u(\lambda)$. By substituting (3.1) into (3.2), the internal form of the filter can be presented as

$$\varepsilon(\lambda) = R_u(\lambda)u(\lambda) + R_d(\lambda)d(\lambda) + R_w(\lambda)w(\lambda) + R_f(\lambda)f(\lambda),\tag{3.4}$$

where $R_u(\lambda)$, $R_d(\lambda)$, $R_w(\lambda)$ and $R_f(\lambda)$ are obtained via

$$[R_u(\lambda) \mid R_d(\lambda) \mid R_w(\lambda) \mid R_f(\lambda)] = Q(\lambda) \begin{bmatrix} G_u(\lambda) & G_d(\lambda) & G_w(\lambda) & G_f(\lambda) \\ I & 0 & 0 & 0 \end{bmatrix}.\tag{3.5}$$

Remark. *The presented internal form of the filter in (3.4) also applies for closed-loop systems [14].*

The fault detector filter $Q(\lambda)$ has to satisfy the following conditions; the decoupling conditions (i, ii), the detection condition for the fault input (iii) and the attenuation condition for the noise input(iv):

$$\begin{aligned}\text{(i)} \quad &R_u(\lambda) = 0, \\ \text{(ii)} \quad &R_d(\lambda) = 0, \\ \text{(iii)} \quad &R_{f_j}(\lambda) \neq 0 \quad j = 1, \dots, m_f, \\ \text{(iv)} \quad &R_w(\lambda) \approx 0.\end{aligned}$$

To satisfy each of the conditions, the factorized representation in (3.6) is used

$$Q(\lambda) = Q_K(\lambda) \dots Q_2(\lambda)Q_1(\lambda),\tag{3.6}$$

where each $Q_i(\lambda)$ has a functionality in achieving these conditions. The fault detection problem is divided into the exact fault detection problem (EFDP) or the approximate fault detection problem (AFDP) and is extended to a fault detection and isolation problem (FDIP), which are described in the sections 3.2 - 3.4.

3.2 Exact fault detection problem

In the exact fault detection problem (EFDP), a filter $Q(\lambda)$ has to be synthesized which only satisfies the conditions i) to iii). Hence, EFDP assumes the noise input is neglectable, i.e., $w = 0$. The section describes the mathematical procedures to obtain such a fault detection filter.

3.2.1 Nullspace method

The nullspace method enable the direct decoupling of both the disturbance d and control input u , and provides minimal order fault detection filters. A left minimal basis matrix $N_l(\lambda)$ with dimensions $(p-r_d) \times (p+m_u)$ can be computed, where $r_d := \text{rank } G_d(\lambda)$, such that $N_l(\lambda)G(\lambda) = 0$. Here, $G(\lambda)$ is defined as

$$G(\lambda) = \begin{bmatrix} G_u(\lambda) & G_d(\lambda) \\ I_{m_u} & 0 \end{bmatrix}.\tag{3.7}$$

Definition 1. (Rank). *The rank of rational matrix $G(\lambda)$, also denoted as normal rank, is the maximum linear independent rows over the field of rational functions $\mathbb{R}(\lambda)$ [8]. In continuous-time, the normal rank of $G(s)$ is the rank of $G(s)$ at all values of s , except for s which cause rank deficiency [15].*

Definition 2. (Basis). $V(\lambda)$ is called a basis of $\mathcal{V}(\lambda)$, where $V(\lambda) := \{v_1(\lambda), v_2(\lambda), \dots, v_k(\lambda)\} \subset \mathcal{V}(\lambda)$. Hence, $\mathcal{V}(\lambda)$ can be constructed with a combination of the rational independent vectors of $V(\lambda)$. In other words, vectors of $V(\lambda)$ are a subset of $\mathcal{V}(\lambda)$ and are linearly independent.

Definition 3. (Minimal basis). Denote n_i being the greatest degree of the i -th row of the polynomial basis. Then the order the polynomial basis, n_d , is equal the sum of the row degrees $n_d = \sum n_i$. The minimal basis is where order n_d is the least.

The method is first introduced in [16], which uses unreliable polynomial manipulation to compute a minimal polynomial basis $N_l(\lambda)$. The method is later extended to minimal rational basis $N_l(\lambda)$ in [17], [18], which relies on pencil reduction algorithms in [19]. These computations rely on state space or descriptor systems representation of the rational matrix $G(\lambda)$ and makes use of orthogonal similarity transformations, which is numerical more reliable.

The method exploits the simple fact that $N_l(\lambda)$ is a nullspace basis of $G(\lambda)$ iff $\begin{bmatrix} M_l(\lambda) & N_l(\lambda) \end{bmatrix}$ is the left nullspace of the system matrix

$$S(\lambda) = \begin{bmatrix} A - \lambda E & B \\ C & D \end{bmatrix}. \quad (3.8)$$

For proof, see [20]. Then, to compute $N_l(\lambda)$, an equivalent left nullspace $Y_l(\lambda)$ is first computed such that $Y_l(\lambda)S(\lambda) = 0$. Hence, $N_l(\lambda)$ is then simply

$$N_l(\lambda) = Y_l(\lambda) \begin{bmatrix} 0 \\ I_p \end{bmatrix}. \quad (3.9)$$

$N_l(\lambda)$ can be computed using the pencil reduction methods. First, the orthogonal matrices Q and Z are determined such that the system matrix S can be transformed in the Kronecker-like staircase form

$$\bar{S}(\lambda) = QS(\lambda)Z = \begin{bmatrix} A_r - \lambda E_r & A_{r,l} - \lambda E_{r,l} \\ 0 & A_l - \lambda E_l \\ 0 & C_l \end{bmatrix}, \quad (3.10)$$

where $A_r - \lambda E_r$ has full row rank, except for value of λ which reduces the rank of $A_r - \lambda E_r$, and the pair $(A_l - \lambda E_l, C_l)$ is observable. By choosing $\bar{Y}_l(\lambda)$ in the form

$$\bar{Y}_l(\lambda) = [0 \mid C_l(A_l - \lambda E_l)^{-1} \mid I], \quad (3.11)$$

the left nullspace of $G(\lambda)$ is then computed via

$$N_l(\lambda) = \bar{Y}_l(\lambda)Q \begin{bmatrix} 0 \\ I_p \end{bmatrix}, \quad (3.12)$$

where the latter part is partitioned such

$$Q \begin{bmatrix} 0 \\ I_p \end{bmatrix} = \begin{bmatrix} B_{r,l} \\ B_l \\ D_l \end{bmatrix}. \quad (3.13)$$

Hence, the descriptor system representation of $N_l(\lambda)$ is then obtained via

$$N_l(\lambda) = C_l(A_l - \lambda E_l)^{-1}B_l + D_l := \left[\begin{array}{c|c} A_l - \lambda E_l & B_l \\ \hline C_l & D_l \end{array} \right]. \quad (3.14)$$

Remark 1. If the system $G(\lambda)$ is minimal, then $N_l(\lambda)$ is a minimal proper rational basis [17].

To determine if the descriptor system $G(\lambda)$ is minimal, the following five conditions, described in [8], have to be checked.

Theorem 1. *A descriptor system $G(\lambda) = C(\lambda E - A)^{-1}B + D$ of order n is minimal iff*

- (a) $\text{rank} [A - \lambda E \quad B] = n,$
- (b) $\text{rank} [E \quad B] = n,$
- (c) $\text{rank} \begin{bmatrix} A - \lambda E \\ C \end{bmatrix} = n,$
- (d) $\text{rank} \begin{bmatrix} E \\ C \end{bmatrix} = n,$
- (e) $A \ker(E) \subseteq \text{Im}(E).$

If the conditions (a, b) are satisfied, the system is controllable. The conditions (c, d) defines the observability of the system. Lastly, if condition (e) is satisfied, then there are no non-dynamics modes present, i.e, no simple infinite eigenvalues.

In case that the disturbance is absent in $G(\lambda)$, i.e., $G_d(\lambda) = 0$, the left minimal basis $N_l(\lambda)$ is simply the full-order Luenberger observer

$$N_l(\lambda) = [I_p \quad -G_u(\lambda)]. \quad (3.15)$$

To check if the computed nullspace basis $N_l(\lambda)$ is a valid as fault detector, the (detectability) condition iii) has to be satisfied. This means the following condition should hold

$$R_f(\lambda) = N_l(\lambda) \begin{bmatrix} G_f(\lambda) \\ 0 \end{bmatrix} \neq 0, \quad (3.16)$$

where $G_f(\lambda)$ is the fault TFM. Let G_{f_j} be the j -th fault (column) of $G_f(\lambda)$. Then a necessary and sufficient condition for the existence of a solution is the following one (from [16])

Theorem 2. *A solution to EFDP exist iff*
 $\text{rank} [G_d(\lambda) \quad G_{f_j}(\lambda)] > \text{rank} G_d(\lambda), j = \{1, \dots, m_f\}.$

Theorem 2 defines if the system in (3.1) is complete fault detectability and the admissibility property of the fault detector filter.

Definition 4. (Complete fault detectable). *The system in (3.1) is complete fault detectable if there exist a fault detection filter $Q(\lambda)$ such that $R_{f_j}(\lambda) = Q(\lambda) [G_{f_j}(\lambda) \quad 0]^T \neq 0, j = \{1, \dots, m_f\}$, i.e., all faults are detectable. The fault detector filter $Q(\lambda)$ is then called admissible.*

Let Ω , be a set of frequencies in which the fault, f , occurs. In case of a persistent fault at frequency Ω , it is desired that the residual signal $\varepsilon(\lambda)$ does not decay. Therefore, the fault condition in (3.16) is extended to a strong fault detection condition.

Definition 5. (Strong fault detectable). *A fault f is strong detectable at frequency Ω by the fault detector filter $Q(\lambda)$, if the corresponding fault-to-residual TFM $R_f(\lambda)$ has no zeros present at Ω , i.e., $R_f(\lambda)$ has a non-zero DC-gain such that $R_f(0) \neq 0$.*

In continuous-time, a common choice for the fault signal is a step $\Omega = \{0\}$, i.e., an abrupt change, or a sinusoidal signal at frequency $\Omega = w_x$, i.e., an evolving fault.

Then, one possible approach to build a stable scalar output detector, that satisfies (3.16), is by building linear combinations of the left minimal nullspace basis such that

$$\bar{N}_l(\lambda) = h(\lambda)N_l(\lambda), \quad (3.17)$$

where $h(\lambda)$ is a row vector. Via the combinations of $h(\lambda)$ all possible fault detectors can be synthesized.

In case the conditions are fulfilled, the detector(s) are updated via $Q_1(\lambda) = N_l(\lambda)$, $R_f(\lambda) = Q_1(\lambda) [G_{f_j}(\lambda) \quad 0]^T$.

3.2.2 Achieving least order detector(s)

Let $Q_1(\lambda) = N_l(\lambda)$. A row vector $Q_2(\lambda)$ has to be computed such that the fault detection filter $Q_2(\lambda)Q_1(\lambda)$ has the desired number of residuals and has the least McMillan degree. This is desired to reduce the computational expense of the filter. An important condition is that $Q_2(\lambda)Q_1(\lambda)$ is admissible, i.e., satisfies the detection condition iii). By employing the minimal dynamic cover techniques in [21], the least order detector(s) can be obtained.

First, a special form of the controllability staircase algorithm, described in [22], is employed on the system matrices in (3.14), such that $Q_2(\lambda)$ can be formulated as

$$Q_2(\lambda) = \left[\begin{array}{c|c} A_l + KC_l - \lambda E_l & K \\ \hline HC_l & H \end{array} \right], \quad (3.18)$$

where the matrices (A_l, C_l, E_l) are based on (3.14). Then $Q_2(\lambda)Q_1(\lambda)$ has the form

$$Q_2(\lambda)Q_1(\lambda) = \left[\begin{array}{c|c} A_l + KC_l - \lambda E_l & B_l + KD_l \\ \hline HC_l & HD_l \end{array} \right], \quad (3.19)$$

where H is a full row rank matrix and K is the output injection matrix. The matrix H is often randomly chosen, i.e., fixed. Then, the matrix K is determined, such that the fault detection filter $Q_2(\lambda)Q_1(\lambda)$ has the least possible McMillan degree and satisfies the admissibility condition. To compute such a matrix K , two nonsingular transformation matrices U and V are computed via the Type 1 dynamic cover algorithm in [21], such that the system is put into a maximum unobservable form to cancel the maximum number of poles. In what follows, describes the computation of the matrix K shortly.

Firstly, the matrices U and V are computed such that

$$U(A_l - \lambda E_l)V = \left[\begin{array}{c|c} \hat{A}_{11} - \lambda \hat{E}_{11} & \hat{A}_{12} - \lambda \hat{E}_{12} \\ \hline \hat{A}_{21} & \hat{A}_{22} - \lambda \hat{E}_{22} \end{array} \right], UB_l = \begin{bmatrix} \hat{B}_1 \\ \hat{B}_2 \end{bmatrix}, \begin{bmatrix} hC_l \\ C_l \end{bmatrix} V = \begin{bmatrix} 0 & \hat{C}_{22} \\ \hat{C}_{11} & \hat{C}_{12} \end{bmatrix}, \quad (3.20)$$

where the pairs $(\hat{A}_{11} - \lambda \hat{E}_{11}, \hat{C}_{11})$ and $(\hat{A}_{22} - \lambda \hat{E}_{22}, \hat{C}_{22})$ are observable. The matrices \hat{C}_{11} and \hat{A}_{21} has the following structure

$$\begin{bmatrix} \hat{A}_{21} \\ \hat{C}_{11} \end{bmatrix} = \begin{bmatrix} 0 & A_{21} \\ 0 & C_{11} \end{bmatrix}, \quad (3.21)$$

where C_{11} has full column rank. By taking

$$K = U^{-1} \begin{bmatrix} 0 \\ K_2 \end{bmatrix}, \quad (3.22)$$

with K_2 satisfying $K_2 C_{11} + A_{21} = 0$, the part $\hat{A}_{21} + K_2 \hat{C}_{11}$ is eliminated. Hence, the eigenvalues in $\hat{A}_{11} - \lambda \hat{E}_{11}$ are unobservable. By removing these unobservable states, the least order fault detector filter $Q_2(\lambda)Q_1(\lambda)$ is obtained.

If $Q_2(\lambda)Q_1(\lambda)$ is of least order and satisfies the admissibility condition, the fault detection filter is updated via $Q(\lambda) = Q_2(\lambda)Q_1(\lambda)$, $R_f(\lambda) = Q_2(\lambda)R_f(\lambda)$.

3.2.3 Enforcing stability and desired dynamics

To synthesize a physically realizable (properness) filter $Q(\lambda)$ and TFM $R_f(\lambda)$, a factor $Q_3(\lambda)$ is employed such that $Q_3(\lambda) \begin{bmatrix} Q(\lambda) & R_f(\lambda) \end{bmatrix}$ are stable and have only poles in a "good" region. This region is defined by the engineer.

For the computation of the factor $Q_3(\lambda)$, the left-coprime factorization (LCF) is used. Via the left co-prime factorization, the filter can be represented as

$$\begin{bmatrix} Q(\lambda) & R_f(\lambda) \end{bmatrix} = Q_3(\lambda)^{-1} \begin{bmatrix} \bar{Q}(\lambda) & \bar{R}_f(\lambda) \end{bmatrix} \quad (3.23)$$

where $[\bar{Q}(\lambda) \ \bar{R}_f(\lambda)]$ and $Q_3(\lambda)$ are stable coprime factors. The stability of both factors implies that $[\bar{Q}(\lambda) \ \bar{R}_f(\lambda)]$ should contain all the RHP-zeros of $[Q(\lambda) \ R_f(\lambda)]$ and $Q_3(\lambda)$ should contain all RHP poles of $[Q(\lambda) \ R_f(\lambda)]$ as RHP-zeros. The coprimeness implies that both factors should have no common RHP-zeros that could cause pole-zero cancellation when forming $Q_3(\lambda)^{-1} [\bar{Q}(\lambda) \ \bar{R}_f(\lambda)]$ [15]. Note, that the order of the filter $Q(\lambda)$ is not increased when employing LCF and keeps the minimal property.

Assume the following descriptor realization

$$[Q(\lambda) \ R_f(\lambda)] = \left[\begin{array}{c|cc} A - \lambda E & B & B_f \\ \hline C & D & D_f \end{array} \right], \quad (3.24)$$

where the poles of $[Q(\lambda) \ R_f(\lambda)]$ relates to $\Lambda(A - \lambda E)$. Via the orthogonal matrices Q and Z , the regular pencil $(A - \lambda E)$ is transformed to a specially ordered generalized real Schur form (GRSF) $(\bar{A} - \lambda \bar{E}) := Q(A - \lambda E)Z$ such that

$$\bar{A} - \lambda \bar{E} = \begin{bmatrix} A_\infty & * \\ 0 & A_{22} - \lambda E_{22} \end{bmatrix}, \quad (3.25)$$

where A_∞ contains all simple infinite eigenvalues of $A - \lambda E$ corresponding to first-order eigenvectors and

$$A_{22} - \lambda E_{22} = \begin{bmatrix} A_g - \lambda E_g & * & * \\ 0 & A_{f,b} - \lambda E_{f,b} & * \\ 0 & 0 & A_{\infty,b} - \lambda E_{\infty,b} \end{bmatrix}, \quad (3.26)$$

where $A_g - \lambda E_g$ contains the stable finite eigenvalues, $A_{f,b} - \lambda E_{f,b}$ contains the unstable finite eigenvalues and $A_{\infty,b} - \lambda E_{\infty,b}$ contains the unstable infinite eigenvalues. Then via the algorithm **GRCF** or **GRCFID** in [23], a factor $Q_3(\lambda)$ is computed which relocates all controllable stable/unstable and finite/infinite eigenvalues to a stable location and removes all uncontrollable eigenvalues. Note, numerically instability can occur when the infinity-norm of the partial feedback gains $\|F_2\|$, which is used to relocate the unstable eigenvalues, is too large. This can happen when unstable eigenvalues are too far in the unstable region or are weakly controllable.

In Fig 3.2, the LCF in continuous-time is visualized. The parameter *smarg* is the threshold value which defines if a pole (eigenvalue) is 'unstable', marked with red cross. This 'unstable' pole can also be a stable pole close to the origin. The 'unstable' poles are then relocated to the desired stable location, given via the parameter *sdeg* or to the location *poles*. The parameter *sdeg*, is a real negative real value and *poles* is a pair of complex negative poles, marked with green crosses.

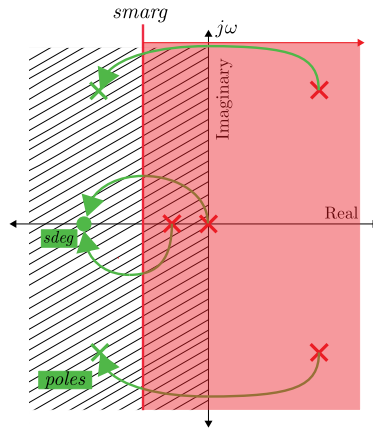


Fig. 3.2: Visualization of the left co-prime factorization. The 'unstable' poles, indicated with red crosses, are moved to the position of *sdeg*, a negative real value, or to the pole locations, indicated with green crosses. The 'unstable' poles are defined by the threshold parameter *smarg*.

After relocating the 'unstable' poles to the 'good' region, the filter is updated via $[Q(\lambda) \ R_f(\lambda)] = Q_3^{-1}(\lambda) [\bar{Q}(\lambda) \ \bar{R}_f(\lambda)]$.

3.3 Approximate fault detection problem

In the approximate fault detection problem (AFDP), a fault detection filter $Q(\lambda)$ has to be synthesized, which satisfies the conditions i) to iv). This includes the attenuation of the noise input $\omega(\lambda)$. However, before the AFDP is solved, the following theorem from [8] is first considered

Theorem 3. *The AFDP is solvable iff EFDP is solvable.*

If the EFDP is not solvable, the disturbance can be reformulated as noise, i.e., $G_w(\lambda) = G_d(\lambda)$. Hence, the EFDP is then, in most cases, solvable.

The procedure of AFDP is similar to the EFDP procedure, such as computing the left minimal basis $N_l(\lambda)$, computing the least order detector(s) and enforcing stabilization/desired dynamics. However, AFDP has to satisfy an extra admissibility condition and has an attenuation step. The extra admissibility condition requires $R_w(\lambda)$ to have full row rank, where

$$R_w(\lambda) = Q_2(\lambda)Q_1(\lambda) \begin{bmatrix} G_w(\lambda) \\ 0 \end{bmatrix}. \quad (3.27)$$

The necessity of this admissibility condition is such that the attenuation step, described in the next subsection, is solvable.

3.3.1 Attenuation of noise

Assuming the fault detector filter $Q_2(\lambda)Q_1(\lambda)$ has the least McMillan degree and both admissibility conditions are satisfied, then the attenuation step is formulated as a standard H_2/H_∞ -norm minimization based ‘‘controller’’ synthesis problem [24]. Let $\gamma > 0$ be an admissible level for the effect of the noise signal $w(t)$ on the residual ε and let β be the optimal fault sensitivity level. Then the minimization goal is to determine a proper and stable $Q(\lambda)$ such that

$$\beta = \max_{Q(\lambda)} \{ \|Q(\lambda)R_f(\lambda)\|_{\infty-} \mid \|Q(\lambda)R_w(\lambda)\|_{\infty} \leq \gamma \}, \quad (3.28)$$

where $\|R_f(\lambda)\|_{\infty-}$ is formulated as

$$\|R_f(\lambda)\|_{\infty-} = \min_{1 \leq j \leq m_f} \|R_{fj}(\lambda)\|_{\infty}. \quad (3.29)$$

The authors in [25], [26] introduced a way to solve this optimization problem based on the $\|R_f(\lambda)\|_{-}$ index. However, this norm is based on singular values and only works for occasions when $m_f \leq p$, i.e., number of faults are equal or less than the number of measurements [8].

To overcome this proble, the $\|R_f(\lambda)\|_{\infty-}$ index is introduced in [27]. The optimal solution is based on a special form of coprime factorization, respectively the inner-outer factorization.

Consider $G(\lambda) \in RH_\infty$, i.e., stable proper rational TFM, then an inner-outer factorization exists

$$G(\lambda) = G_i(\lambda)G_o(\lambda) \quad (3.30)$$

where $G_i(\lambda)$ is inner, i.e., $G_i(\lambda)^*G_i(\lambda) = I$. Additionally, $G_i(s)^* = G_i(-s)^T$ in continuous-time and $G_i(s)^* = G_i(1/z)^T$ in discrete-time. The role of the inner factor is to relocate all the RHP zeros of $G(\lambda)$ to $G_i(\lambda)$. An important property of inner (and simultaneously co-inner) is that $G_i(s)$ is an all-pass filter. $G_o(\lambda)$ is outer, i.e., full row rank and only having stable zeros.

In [28], the problem is extended to a quasi-outer-inner [29], which is able to cope with systems having zeros on the boundary of the stability domain. The quasi-outer-inner factorization is formulated as

$$\bar{G}(\lambda) = \bar{G}_o(\lambda)\bar{G}_i(\lambda), \quad (3.31)$$

where $\bar{G}_i(\lambda)$ is still inner. The result is that $\bar{G}_o(\lambda)$ may now contain zeros which lie on the boundary of the stability domain.

Consider again the optimization problem (3.28). The importance of $R_w(\lambda)$ in (3.27) to have the full row rank property, is due to the full row rank requirement of solving the Ricatti equation

(CARE) in the quasi-outer-inner factorization. The full details on the computation can be found in [29]. Assuming R_w to have full row rank, then the quasi-outer-inner factorization of R_w is

$$R_w(\lambda) = R_{wo}(\lambda)R_{wi}(\lambda). \quad (3.32)$$

Substituting R_w in (3.28) with the factorization above gives

$$\beta = \max\{\|Q(\lambda)R_f(\lambda)\|_{\infty-} \mid \|Q(\lambda)R_{wo}(\lambda)R_{wi}(\lambda)\|_{\infty} \leq \gamma\}. \quad (3.33)$$

Using the all-pass inner property of $R_{wi}(\lambda)$, i.e., $R_{wi}(\lambda) = I$, simplifies the optimization problem to

$$\beta = \max\{\|Q(\lambda)R_f(\lambda)\|_{\infty-} \mid \|Q(\lambda)R_{wo}(\lambda)\|_{\infty} \leq \gamma\}. \quad (3.34)$$

Then by choosing $Q(\lambda) = Q_5(\lambda)Q_4(\lambda)Q_3(\lambda)$, where $Q_3(\lambda) = R_{wo}(\lambda)^{-1}$, the problem is formulated as

$$\beta = \max\{\|Q_5(\lambda)Q_4(\lambda)R_{wo}(\lambda)^{-1}R_f(\lambda)\|_{\infty-} \mid \|Q_5(\lambda)Q_4(\lambda)\|_{\infty} \leq \gamma\}. \quad (3.35)$$

In case $R_w(\lambda)$ has no zeros present in the origin, the optimization problem is simplified by choosing the constant matrices $Q_4 = I$ and a scalar matrix $Q_5 = \Psi I$, such that the requirements $\|Q_5(\lambda)Q_4(\lambda)\|_{\infty} \leq \gamma$ is satisfied.

If $R_w(\lambda)$ has zeros present in the origin, then $Q_3(\lambda) = R_{wo}(\lambda)^{-1}$ could lead to an unstable filter $Q(\lambda)$. Via LCF, a factor $Q_4(\lambda)$ is constructed which stabilizes the filter $Q(\lambda)$ and enforces the desired dynamics by relocating the unstable poles. Then a constant matrix $Q_5(\lambda) = \Psi I$ is chosen to satisfy $\|Q_5(\lambda)Q_4(\lambda)\|_{\infty} \leq \gamma$ is satisfied.

3.4 Fault detection and isolation problem

The fault detection and isolation problem (FDIP) extends the problem to the localization of faulty actuators or sensors. It therefore uses a bank of scalar fault detectors. The detectors are shaped via the binary matrix, S , which has dimensions of $q \times m_f$, where q is the number of residuals and m_f the number of faults. This matrix S is chosen, such that the following condition from [8] is fulfilled:

$$S_{R_f} = S, \text{ with } R_f(\lambda) \text{ stable} \quad (3.36)$$

In other words, the TFM $R_f(\lambda)$ has the same structure as the binary matrix S . To check if the condition above is solvable, the following theorem from [8] can be used:

Theorem 4. For a given $q \times m_f$ binary matrix S , the system in (3.1) is S -fault isolatable iff for $i = 1, \dots, q$

$$\text{rank} \begin{bmatrix} G_d & \bar{G}_d^{(i)} & G_{f_j} \end{bmatrix} > \text{rank} \begin{bmatrix} G_d & \bar{G}_d^{(i)} \end{bmatrix}, \forall j, S_{ij} \neq 0, \quad (3.37)$$

where $\bar{G}_d^{(i)}$ is formed from the columns of G_f for which $S_{ij} = 0$.

Ideally, the detection of simultaneously faults is desired, called strong isolatable. This requires the system to be S -fault isolatable with $S = I_{m_f}$. However, this is not always achievable due to the lack of sufficient number of measurement or due to the system characteristics.

To enforce $R_f(\lambda)$ to have the same structure as S , a factor $\bar{Q}_1(\lambda)$ is introduced, such that

$$Q(\lambda) = \bar{Q}_1(\lambda)Q_1(\lambda). \quad (3.38)$$

Then, for every i -th row of S , a fault detector $\bar{Q}_1^{(i)}(\lambda)$ is computed via EFDP or AFDP, such that j -th fault (column) of $|R_{f_j}(\lambda)| = 0, S_{ij} = 0$ and $|R_{f_j}(\lambda)| \neq 0, S_{ij} = 1$. To achieve $|R_{f_j}(\lambda)| = 0$, the column is reformulated as a disturbance input and decoupled via the nullspace methods, i.e., $\bar{G}_d(\lambda) = R_{f_j}(\lambda)$.

Chapter 4

Design freedom and limitation

This chapter described the design freedom and limitation of the nullspace-based fault diagnosis on high-tech precision systems. Additionally, an overview of the limitation is given.

4.1 Design freedom

To synthesis the fault detector $Q(\lambda)$, the nullspace-based fault diagnosis has synthesis options that have to be designed by the engineer. This section, describes the design options which are considered important for high-precision systems.

4.1.1 Disturbances characterization in motion systems

The disturbances in high-tech precision systems are often assumed to be low-frequent and stochastic. In conventional control, these disturbances are dealt with by frequency-based PID controllers. Therefore, disturbance models are not commonly used. Hence, $G_d(\lambda)$ is assumed to be zero.

4.1.2 Nullspace computations

Considering the assumption that disturbance models are absent, the computation of the left nullspace $N_l(\lambda)$ is simply the full Luenberger observer. However, when dealing with systems having poles at $\Omega = \{0\}$, e.g., an unsuspended system, the use of the Luenberger observer did not prove to be numerically reliable, since $R_u(\lambda) = 0$ was not satisfied.

Therefore, it is recommended to compute the left nullspace via the pencil reduction methods, described in Chapter 3, which is proven to be numerically more reliable.

4.1.3 Noise characterization in motion systems

In high-tech systems, the noise is often assumed to be either high frequent, or white, i.e., equal presence of all frequencies over the entire frequency spectrum. Therefore, the noise model $G_w(\lambda)$ is modelled as either an all-pass or as a high-pass filter. Considering the inner-outer factorization in (3.31), the all-pass noise model can be represented by two inner terms, i.e., all-pass filters. Therefore, this noise model has no effect on the minimization problem in (3.33). Hence, the use of an all-pass filter as noise model for fault diagnosis is impractical.

4.1.4 Pole instability threshold *smarg*

In the synthesis, the parameter *smarg* is available for design. This parameter determines which poles in $Q(\lambda)$ are considered 'unstable'. In this case, the term 'unstable' can also include slow stable poles. By relocating these poles via the left coprime factorization, the response speed of $Q(\lambda)$ is regulated. Increasing *smarg* relocates more poles and increases the response speed of $Q(\lambda)$. However, this may result in numerical issues due to the requirement of a high feedback gain for a weakly controllable pole.

4.1.5 Pole relocation *sdeg*

In the synthesis, the parameter *sdeg* is available for design. This parameter is the negative real-part pole location to which the 'unstable' poles in $Q(\lambda)$ are relocated to. In other words, *sdeg* also regulated the speed of the $Q(\lambda)$. However, if *sdeg* is a pole location which is hard to reach for some weakly 'unstable' controllable poles, a high partial feedback gain is required. This can result in numerical instabilities.

4.1.6 Minimality

Via the minimality option, the least order detector(s) can be computed via the minimum dynamic cover technique. However, this technique uses non-orthogonal transformation matrices, which can introduce numerical issues. Additionally, the strong fault detection property can be lost when combining the basis vectors, see example in Appendix A.

In case of the availability of sufficient computational power, it is better to use the full order design instead of the employing minimality. The full order design outputs all the basis vectors from the left nullspace. Therefore, the full order design could provide better detector candidates, which maintain the strong fault detection property. It is then up to the engineer, to choose the basis vectors via the matrix $h(\lambda)$ in (3.17).

4.2 Limitation on fault isolation

Consider the MIMO parametric model $G_u(\lambda) \in \mathbb{R}(\lambda)^{p \times m_u}$, where p is the number of sensors and m_u the number of control inputs. Assuming that the model is obtained from a high-tech positioning system, it can be denoted as

$$G_u(\lambda) = N(\lambda)/d(\lambda), \quad (4.1)$$

where $N(\lambda)$ is a TFM of numerators and $d(\lambda)$ is their common denominator. In case that both actuator and sensor faults have to be detected, the fault TFM $G_f(\lambda)$ can be written as

$$G_f(\lambda) = [G_u(\lambda) \quad I_p]. \quad (4.2)$$

By substituting (4.1) into (4.2) and factoring out $d(\lambda)$, the fault TFM $G_f(\lambda)$ can be formulated as

$$G_f(\lambda) = [N(\lambda)/d(\lambda) \quad I_p] = \frac{1}{d(s)} [N(\lambda) \quad d(\lambda)], \quad (4.3)$$

which can be written as

$$G_f(\lambda) = \frac{1}{d(s)} \begin{bmatrix} N_{11}(\lambda) & \cdots & N_{1m_u}(\lambda) & d(\lambda) & \cdots & 0 \\ \vdots & \ddots & \vdots & \vdots & \ddots & \vdots \\ N_{p1}(\lambda) & \cdots & N_{pm_u}(\lambda) & 0 & \cdots & d(\lambda) \end{bmatrix}. \quad (4.4)$$

Now recall the decoupling and fault detection conditions in the nullspace-based fault diagnosis, which are

$$[R_u(\lambda) \quad R_d(\lambda)] = Q(\lambda) \begin{bmatrix} G_u(\lambda) & G_d(\lambda) \\ I_{m_u} & 0 \end{bmatrix} = 0, \quad (4.5)$$

and

$$R_f(\lambda) = Q(\lambda) \begin{bmatrix} G_f(\lambda) \\ 0 \end{bmatrix} \neq 0, \quad (4.6)$$

where $Q(\lambda) := [Q_y(\lambda) \quad Q_u(\lambda)]$ is the fault detection filter. Then to decouple the control input u and disturbance input d in (4.5), the following must hold

$$Q_y(\lambda)G_u(\lambda) + Q_u(\lambda)I_{m_u} = 0, \quad (4.7)$$

and

$$Q_y(\lambda)G_d(\lambda) = 0. \quad (4.8)$$

Based on (4.7), the filter part $Q_u(\lambda)$ can be formulated as

$$Q_u(\lambda) = -Q_y(\lambda)G_u(\lambda). \quad (4.9)$$

By substituting (4.9) into (4.6) results in the fault-to-residual TFM

$$R_f(\lambda) = [Q_y(\lambda) \quad Q_u(\lambda)] \begin{bmatrix} G_f(\lambda) \\ 0 \end{bmatrix} = Q_y(\lambda) [I_p \quad -G_u(\lambda)] \begin{bmatrix} G_f(\lambda) \\ 0 \end{bmatrix} = Q_y(\lambda)G_f(\lambda) \neq 0. \quad (4.10)$$

Now assume $G_d(\lambda) = 0$. A simple possible solution for the filter $Q(\lambda)$ that satisfies the conditions (4.5) and (4.6), is by choosing $Q_y(\lambda) = I_p$, which corresponds to the full Luenberger observer in (3.15). Substituting this solution for $Q_y(\lambda)$ in (4.10) results in

$$R_f(\lambda) = G_f(\lambda) \neq 0. \quad (4.11)$$

Now consider that the detection problem is extended to an isolation problem, i.e., localization of the faults. Therefore, a binary structure matrix S with dimension $q \times m_f$ is introduced, where m_f are the number of faults and q the number of residuals. To enforce the fault-to-residual $R_f(\lambda)$ to have the same structure as S , the transfer function $\bar{Q}_y(\lambda)$ is introduced such that

$$\bar{Q}_y(\lambda)R_f(\lambda) = \bar{R}_f(\lambda), \quad (4.12)$$

where $\bar{R}_f(\lambda)$ has the same structure as S .

Notation: For the notation of the row vectors of a transfer matrix, a superscript is used, e.g.,

$$R(s) = \begin{bmatrix} R^1(s) \\ \vdots \\ R^p(s) \end{bmatrix} = \begin{bmatrix} R_{11}(s) & \dots & R_{1m_u}(s) \\ \vdots & \dots & \vdots \\ R_{p1}(s) & \dots & R_{pm_u}(s) \end{bmatrix}. \quad (4.13)$$

For convenience, a single row of S is considered. This simplifies (4.12) to find a single row vector $\bar{Q}_y^1(\lambda)$ such that

$$\bar{Q}_y^1(\lambda)R_f(\lambda) = \bar{R}_f^1(\lambda). \quad (4.14)$$

Then recall that $R_f(\lambda) = G_f(\lambda)$ in (4.11). Hence, (4.14) can be formulated as

$$\underbrace{\begin{bmatrix} \bar{Q}_{y_1}^1(\lambda) \\ \vdots \\ \bar{Q}_{y_p}^1(\lambda) \end{bmatrix}}_{\bar{Q}_y^1(\lambda)} \frac{1}{d(s)} \underbrace{\begin{bmatrix} N_{11}(\lambda) & \dots & N_{1m_u}(\lambda) & d(\lambda) & \dots & 0 \\ \vdots & \ddots & \vdots & \vdots & \ddots & \vdots \\ N_{p1}(\lambda) & \dots & N_{pm_u}(\lambda) & 0 & \dots & d(\lambda) \end{bmatrix}}_{R_f(\lambda)} = \underbrace{[\bar{R}_1^1(\lambda) \quad \dots \quad \bar{R}_{m_f}^1(\lambda)]}_{\bar{R}_f^1(\lambda)}, \quad (4.15)$$

where the j -th column (fault) of $|\bar{R}_j^1(\lambda)| = 0$ when $S_j^1 = 0$ and $|\bar{R}_j^1(\lambda)| \neq 0$, when $S_j^1 = 1$. Based on (4.15), the following constraints can be formulated:

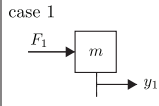
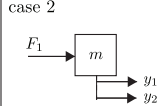
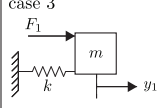
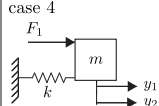
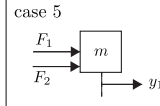
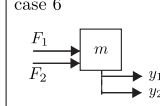
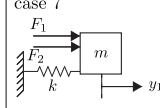
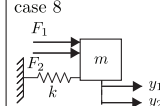
- There exists no solution for the filter part $\bar{Q}_y^1(\lambda)$ if all sensors are decoupled. To satisfy $\bar{Q}_{y_i}^1(\lambda)d(\lambda) = 0 \quad \forall i \in \{1, \dots, p\}$, results in $\bar{Q}_y^1(\lambda) = 0$. Hence, $\bar{Q}_y^1(\lambda)R_f(\lambda) = 0$, which means that all the faults are undetectable.
- The detectability and isolability of $\bar{Q}_y^1(\lambda)$, is limited to the linear independency of the numerator TFM $N(\lambda)$ of $G_u(\lambda)$. Decoupling a column of $N(\lambda)$ via $\bar{Q}_y^1(\lambda)$ can result in decoupling of other columns of $N(\lambda)$, see example in Appendix B.

4.3 Overview

For the detection and localization of both actuator and sensor faults, it is desirable to synthesize a fault detection filter $Q(\lambda)$ that has the strong fault detectability and isolability property. In particular, the faults have to be strong fault detectable at $\Omega = \{0\}$, such that persistent faults do not decay in the residuals. An overview of possibilities and limitation of the nullspace-based fault diagnosis for both suspended and unsuspended systems is depicted in Fig 4.1.

Remark. *In this section, only mass and mass-spring systems are considered for $G_u(s)$, e.g., $\frac{1}{s^2}$ for unsuspended systems or $\frac{1}{s^2+k}$ for suspended systems. Hence, systems with dampers and/or flexible modes are not considered.*

Assumption. *The force(s) introduced in the system do not introduce rotation.*

	strong fault detectable at $\Omega = \{0\}$		isolatable	
	actuator(s)	sensor(s)	actuator(s)	sensor(s)
case 1 	😊	😞	😞	😞
case 2 	😊	😊	😊	😞
case 3 	😊	😊	😞	😞
case 4 	😊	😊	😊	😊
case 5 	😊	😞	😞	😞
case 6 	😊	😊*	😞*	😞
case 7 	😊	😊	😞	😞
case 8 	😊	😊	😞*	😊*

* In case of a small change in the transfer TFM, e.g., $G_u(s) = \begin{bmatrix} \frac{1}{s^2} & \frac{2}{s^2} \end{bmatrix}$, the properties do not apply anymore, see Appendix E

Fig. 4.1: The possibility and limitation of the nullspace-based fault diagnosis for the detection and isolation of actuator and sensor faults on suspended and unsuspended systems. In case of a footmark, the system has to satisfy linear dependency conditions.

First to observe, is that in a system where only one measurement is available, the filter $Q(\lambda)$ is unable to isolate the faults. Since only one measurement is available, the left nullspace basis has only one vector available, resulting in $R_f(\lambda)$ having only a single row vector. Hence, there does not exist a factor $\bar{Q}_y^1(\lambda)$ in (4.14), such that $\bar{Q}_y^1(\lambda)R_f(\lambda)$ decouples one fault without decoupling the other fault.

Secondly, the sensor faults in unsuspended system are not always strong fault detectable by filter $Q(\lambda)$, see case 6 in Fig 4.1. Recall that an unsuspended system has poles at Ω , i.e., $s = 0$. The consequence is that these unstable poles are cancelled by introducing zeros in $Q(\lambda)$ at Ω , during the LCF procedure. This results in the loss of strong fault detectability property of $Q(\lambda)$ for sensor faults. However, if the rows in the numerator TFM $G_u(\lambda)$, are linear dependent, then a nullspace basis with constant values can be obtained that cancel the poles at $s = 0$, without introducing zeros in $Q(\lambda)$ at $\Omega = \{0\}$. An example is given in Appendix C. The disadvantage of linear dependency among the rows of $G_u(\lambda)$, is the limitation of isolability of actuator faults.

Let $G_u(\lambda) \in \mathbb{R}(\lambda)^{2 \times 2}$ have two columns that are linear dependent. Then the fault TFM $G_f(s)$ has the property

$$\text{rank} \begin{bmatrix} G_{f_1} & G_{f_2} \end{bmatrix} = 1, \quad (4.16)$$

where G_{f_1} and G_{f_2} are the actuator faults. To isolate the two actuators faults, one of the actuators is reformulated as disturbance and then decoupled, e.g., $\tilde{G}_d = G_{f_1}$. However, this does not satisfy the condition in **Theorem 4** (assuming that $G_d = 0$). Hence, the actuator faults are not isolatable in this case. This also applies for the isolability of the actuator and sensor faults in case 8, see Fig 4.1.

Remark. *The loss of isolability of the actuators faults, in the event of strong fault detectability for sensor faults, does not apply for a system $G_u(\lambda)$ that contains zeros.*

Chapter 5

Towards fault diagnosis oriented models

For the model-based fault diagnosis approach, an accurate model is key. This chapter describes in which frequency range model accuracy is required, such that the models are suitable for fault diagnosis. In particular, models that are suitable for fault diagnosis in high-tech precision systems.

5.1 Models in high-precision systems

The present state-of-the-art MIMO high-precision systems are difficult to model via first model principles due to their complexity. Hence, data-driven techniques, such as system identification, are developed to obtain accurate models over a certain frequency range. Via the system identification procedure, a non-parametric frequency response function (FRF) is obtained that accurately describes the input-output interconnection within the system. Then a parametric model is fitted on the FRF, as described in [30]. In the coming sections, it is addressed in which frequency range accurate models are required for effective fault diagnosis.

5.2 Models for fault diagnosis

Consider the closed-loop (MIMO) system, including the nullspace-based fault diagnosis system, depicted in Fig 5.1. The nullspace-based fault diagnosis uses the approximate models of the plant G_u , the disturbance G_d , the noise G_w and the fault G_f to synthesis a fault detector Q that outputs a residual ε . The coming subsections investigate the effect of these approximate models on the residual ε . Therefore, the transfers from the inputs r, d, w and f to the residual ε are derived. For simplicity, the continuous-time notation is used. *Note, the full derivation of the transfer functions can be found in Appendix D.*

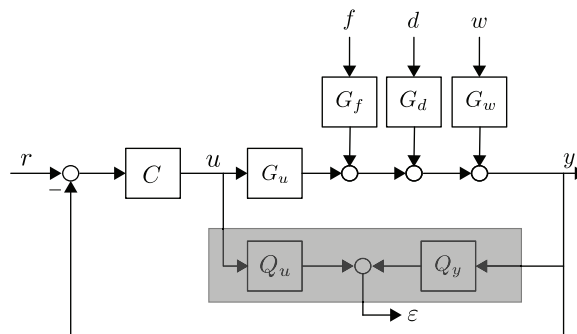


Fig. 5.1: Closed-loop MIMO system including the fault detector filter $Q := [Q_y \ Q_u]$ in (■). The residual ε indicates the presence or absence of the fault input f .

5.2.1 Plant model

This subsection, investigates the effect of modelling errors in the approximate model of plant G_u . Let G_u be the true MIMO system and $\hat{G}_u(s)$ the approximate MIMO model obtained via system identification. Consider the transfer function from reference r to the residual ε in (5.1)

$$T_{\varepsilon r} = Q_y(s)(G_u - \hat{G}_u(s))CS, \quad (5.1)$$

where C is the controller, $Q_y(s)$ is part of the filter $Q(s)$ and S is the sensitivity function $(I + G_u C)^{-1}$. Observe, that the model error is factorized by the control sensitivity CS , which attenuates model errors present in the lower and higher frequency regions. To fully decouple the reference r from residual ε , the following should hold

$$\hat{G}_u(s) = G_u, \quad \forall s, \quad (5.2)$$

as this results in $T_{\varepsilon r} = 0$. However, in practice this does not hold, resulting in the presence of reference signals in the residual. Consider the following assumption made for high-precision systems

Assumption 1. *It is assumed that the reference trajectory for position tracking in high-precision systems has most of the energy at the lower frequencies [31].*

A common choice for position tracking in high-precision systems, is a third or fourth order motion profile where the position profile has a smooth s-curve, depicted in Fig 5.2. Increasing the order of the motion profile reduces the sudden changes in velocity, which decreases the energy content at higher frequencies [32]. Thus, considering Assumption 1, most of the energy of reference

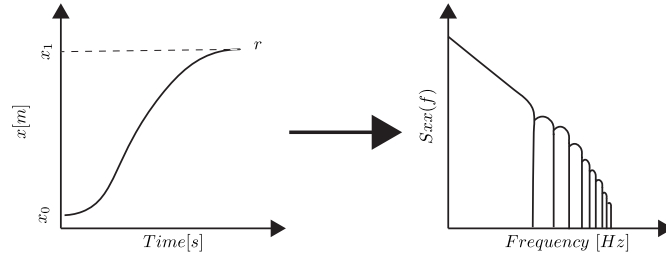


Fig. 5.2: Common third or fourth order reference trajectory and its power density function in motion systems.

r is at the lower frequencies. Hence, to minimize the presence of reference r in residual ε , the approximate model $\hat{G}_u(s)$ should be accurate in this frequency region.

One way to obtain such a model of $\hat{G}_u(s)$ is by weighting this region of frequencies during the system identification [33]. The resulting FRF can then be used as input for local parametric modeling (LPM) [34]. This generates a parametric model $\hat{G}_u(s)$, which can be used for model-based fault diagnosis.

5.2.2 Disturbance model

This subsection, investigates the effect of modelling errors in the approximate model of G_d . Consider the transfer function from the disturbance input d to residual ε in (5.3)

$$T_{\varepsilon d} = Q_y(s)(G_u - \hat{G}_u(s))(-CSG_d) + Q_y(s)G_d. \quad (5.3)$$

Observe that the model error in $\hat{G}_u(s)$ also influences the transfer function of $T_{\varepsilon d}$. Depending on the frequency-spectrum of the disturbance signal d , the approximate model $\hat{G}_u(s)$ should be accurate in this range of frequencies. In high-tech systems, the disturbance d is often assumed to be low-frequent and stochastic. Hence, the approximate model \hat{G}_d should be accurate in the lower-frequencies. However, due to the stochastic property of d , it is impossible for the filter part $Q_y(s)$ to fully decouple d .

5.2.3 Noise model

This subsection, investigates the effect of modelling errors in the approximate model of G_w . Consider the transfer function from the noise input w to residual ε in (5.4)

$$T_{\varepsilon w} = Q_y(s)(G_u - \hat{G}_u(s))(-CSG_w) + Q_y(s)G_w. \quad (5.4)$$

The model error in $\hat{G}_u(s)$ is also traced back into the transfer of $T_{\varepsilon w}$. In this case, the noise $w(\lambda)$ is assumed to be stochastic and high-frequent in high-precision systems. Hence, the approximate model $\hat{G}_w(s)$ has to be accurate in the higher frequency-spectrum.

5.2.4 Fault model

This subsection, investigates the effect of modelling errors in the approximate model of G_f . Consider the transfer function from the fault input f to residual ε in (5.5)

$$T_{\varepsilon f} = Q_y(s)(G_u - \hat{G}_u(s))(-CSG_f) + Q_y(s)G_f. \quad (5.5)$$

With the assumption that model errors are absent in $\hat{G}_u(s)$, the transfer function is simplified to

$$T_{\varepsilon f} = Q_y(s)G_f. \quad (5.6)$$

In this case, the approximate model $\hat{G}_f(s)$ is not visible in the transfer function. This is due to the requirement that the residual ε is sensitive to the fault input f , i.e., $T_{\varepsilon f} \neq 0$. Nevertheless, it can be assumed that the approximate model $\hat{G}_f(s)$ has to be accurate in the frequency spectrum of the fault signal f , which depends on the type of fault (abrupt changing or a slow varying fault).

Additionally, modelling errors in \hat{G}_f can result in the loss of the strong fault detectability property of the filter $Q(s)$ at $\Omega = \{0\}$. In case that the poles of \hat{G}_f at Ω are modelled incorrectly, it is possible that the fault input f , introduced via G_f , is not strong fault detectable. This is caused by the stabilization step in the synthesis, which introduces zeros in $Q(s)$ at Ω to cancel the unstable poles of \hat{G}_f at Ω , see example below. Hence, for strong fault detectability at $\Omega = \{0\}$, it is important that $\hat{G}_f(s)$ is accurate in Ω .

Example: Consider the following system, $G_u(s) = 0$, $G_d(s) = 0$, $G_w(s) = 0$, $\hat{G}_f(s) = \frac{1}{s^2}$ and $G_f(s) = \frac{1}{s^2+1}$. Here, $\hat{G}_f(s)$ is an approximate model of $G_f(s)$ with a model error at $\Omega = \{0\}$. For example, the stable and proper fault detector

$$Q(s) = \frac{s^2}{(s+1)(s+1)},$$

achieves

$$R_u(s) = 0, \quad R_d(s) = 0, \quad R_w(s) = 0, \quad \hat{R}_f(s) = Q(s)\hat{G}_f(s) = \frac{1}{(s+1)(s+1)}.$$

Observe that $\hat{R}_f(s)$ has no zeros in Ω . Hence, the fault input f is strong fault detectable by $Q(s)$. However, employing the synthesized filter $Q(s)$ on the fault model $G_f(s)$, results in

$$R_f(s) = Q(s)G_f(s) = \frac{s^2}{s^4 + 2s^3 + 2s^2 + 2s + 1}.$$

Observe that $R_f(s)$ has now two zeros at Ω . Hence, in application, the fault input f is not strong fault detectable by $Q(s)$.

Chapter 6

Application to high-tech precision systems

In this chapter, a proof of principle of the nullspace-based fault diagnosis is presented on a suspended system (beam setup) and an unsuspended system (OAT). The first case-study employs the nullspace-based fault diagnosis to detect actuator and sensor faults on both the beam setup and OAT. The second case-study employs the nullspace-based fault diagnosis to decouple virtual cable slab interference present in the OAT.

6.1 Detecting actuator and sensors faults for suspended systems

6.1.1 Experimental beam setup

The beam setup contains three current-driven voice-coil actuators and five fibreoptic sensors. The fibreoptic sensors have a resolution of approximately $1 \mu\text{m}$, and the system has a sample frequency of 4096 Hz. In this case-study, the actuators u_1 , u_2 and u_3 and the sensors y_1 , y_2 and y_3 are considered, see Fig 6.1.

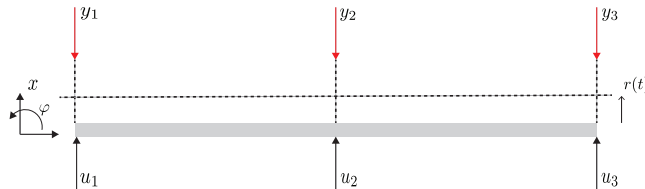


Fig. 6.1: Schematic top view of the beam setup. The flexible beam has three actuators (—). Over the length of the beam, there are three sensors (—) that measure the deformation of the beam.

To obtain a parametric model for fault diagnosis, a non-parametric model is firstly obtained via an open-loop multi-sine system identification. Then via parametric fitting, using the Sanathanan-Koerner and Levenberg-Marquart algorithm, a 10-th order MIMO model $\hat{G}_u(s)$ is obtained, see Fig 6.2. For control purposes, the system is decoupled via the matrices T_u and T_y , such that the modal system is $G_u^{mod} = T_y G_u T_u$. A decentralized controller is employed, and a third order setpoint is injected into the rigid loop. The reference for the rigid body has a maximum amplitude of 0.2 mm.

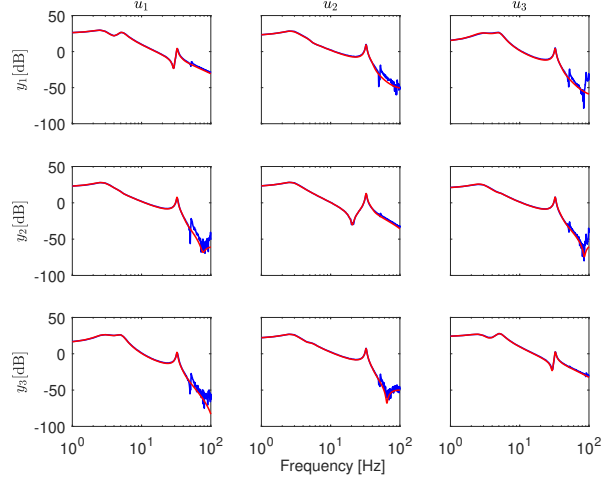


Fig. 6.2: The 10-th order model $\hat{G}_u(s)$ (—) fitted on the measured frequency response function (---) of the beam setup.

6.1.2 FDI design beam setup

The closed-loop system of the beam setup, including the fault detection and isolation (FDI) filters $Q(s)$ and the actuator/sensor fault injections, are depicted in Fig 6.3. Note, that the faults are abrupt changes, i.e., step response, or evolving/varying changes, i.e., ramp or sinusoidal response, which are injected consecutively.

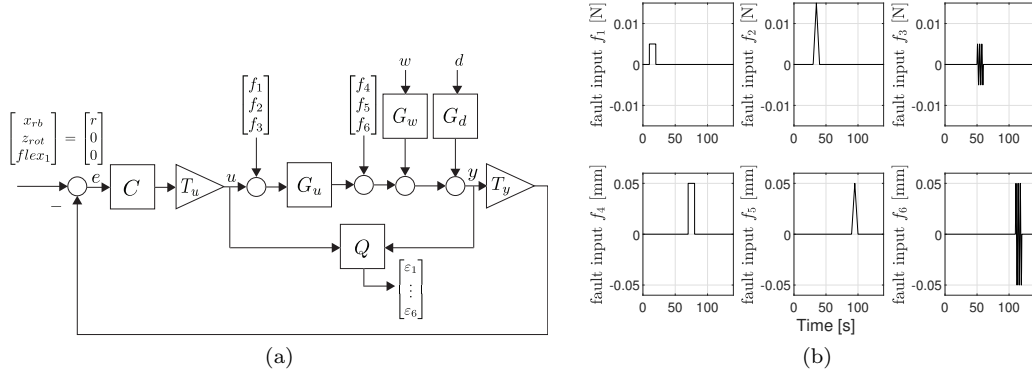


Fig. 6.3: On the left side, the closed-loop control scheme of the beam setup including the employed FDI filters Q and the fault injections. The residuals ε indicate the presence or absence of the actuator/sensor faults f , which are depicted on the right side.

To detect and localize these 6 faults (3 actuator and 3 sensor faults), a bank of filters $Q(s) \in \mathbb{R}(s)^{6 \times 6}$ is synthesized based on the 10-th order model $\hat{G}_u(s)$. Therefore, both the algorithms EFDIP and AFDIP in [35] are employed, which use the synthesis approach as in Chapter 3, to synthesize $Q(s)$. The following design parameters are used: $G_u(s) = \hat{G}_u(s)$, $G_d(s) = 0$, $G_w(s) = \frac{2*s+0.01732}{s+173.3} I_3$, **smarg** = -1, **sdeg** = -3, **nullspace** = true, **minimal** = true, **SFDI** = $S^{6 \times 6}$, **tol** = $1e^{-6}$. In addition, a low-pass filter of $\frac{1}{s+3}$ is employed on the FDI filters to remove any undesired direct-feedthrough terms.

Remark 1. The rank tolerance option in the algorithms is set to $1e^{-6}$ to prevent numerical issues.

$$S^{6 \times 6} = \begin{bmatrix} 0 & 1 & 1 & 1 & 1 & 1 \\ 1 & 0 & 1 & 1 & 1 & 1 \\ 1 & 1 & 0 & 1 & 1 & 1 \\ 1 & 1 & 1 & 0 & 1 & 1 \\ 1 & 1 & 1 & 1 & 0 & 1 \\ 1 & 1 & 1 & 1 & 1 & 0 \end{bmatrix}. \quad (6.1)$$

The fault-to-response TFMs $R_f(s)$, based on the synthesized $Q(s)$ of both algorithms, are depicted in Fig 6.4. The fault inputs f_1, f_2, f_3 are the actuator faults u_1, u_2, u_3 and fault inputs f_4, f_5, f_6 are the sensor faults y_1, y_2, y_3 , respectively. Observe that the TFMs of $R_f(s)$ has the same structure as the binary matrix S .

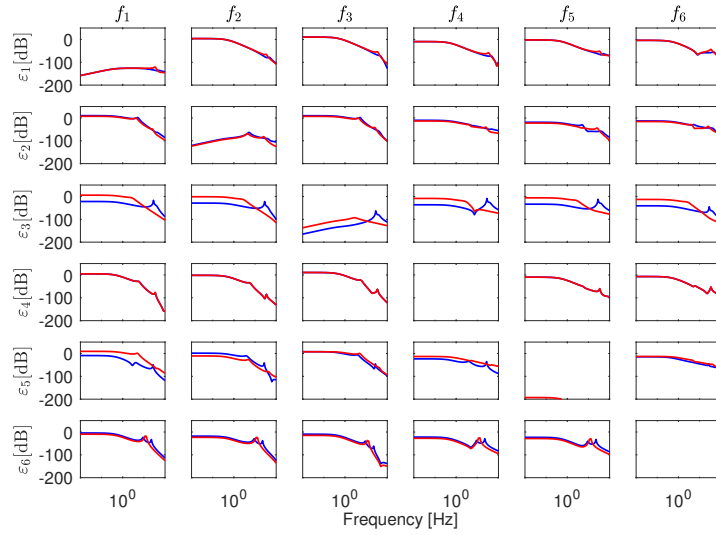


Fig. 6.4: The resulting fault-to-residual TFMs $R_f(s)$ of the EFDISYN algorithm (—) and AFDISYN algorithm (—). Both filters are synthesized on the 10-th order model $\hat{G}_u(s)$. Observe that the AFDISYN algorithm (—) cuts off the higher-frequencies to attenuate the high-frequency noise components. The range of frequencies is from 0.01 Hz to 100 Hz.

6.1.3 Result

The residual signals of the employed FDI filters $Q(s)$ are depicted in Fig 6.5. For clarification, three FDI filters are employed:

1. EFDIP generated filters $Q^a(s)$, employed experimental.
2. AFDIP generated filters $Q^b(s)$, employed experimental.
3. EFDIP generated filters $Q^c(s)$, employed in simulation.

Remark. The generated filters $Q^c(s)$ are based on a 6-th order model $\hat{G}_u(s)$ due to stability issues in simulation. However, for illustration purposes, this difference in order has no effect.

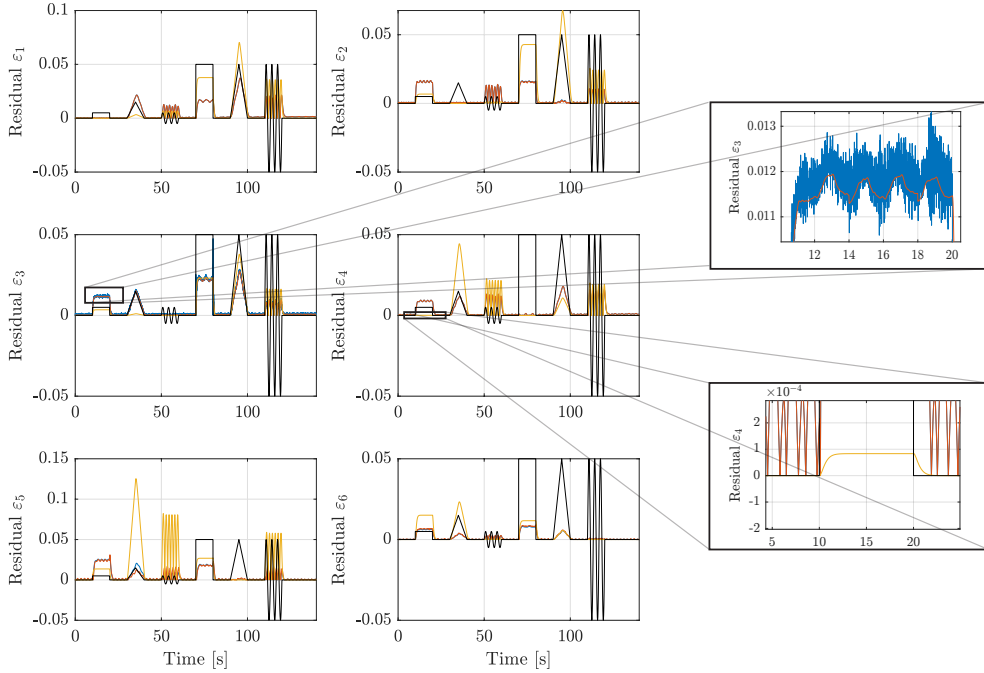


Fig. 6.5: Comparison of the residual signals of the FDI filters $Q^a(s)$, $Q^b(s)$ and $Q^c(s)$, (—),(—),(—), respectively. All the residuals are able to detect the injected actuators and sensors faults (—). The residual signals are further processed by taking the absolute value and averaging. Due to model imperfection, the reference r is not fully decoupled and is present in the experimental employed filters (—), (—). Additionally, the noise effect is reduced by employing the AFDISYN algorithm (—).

First, it is observed that the residuals ε_i for $i = \{1, \dots, 6\}$, do not respond to the fault f_j , where $i = j$. This is enforced via the binary matrix S . In addition, some faults are difficult to see in the residuals. This is in line with the responses in Fig 6.4, where some fault-to-residual transfers are below 0dB. However, by zooming in, it can be seen that the faults are still present in the residuals and non-vanishing, e.g., fault f_1 in residual ε_4 .

Next, it is observed that the reference r is still present in the residuals of the experiments (—),(—). Due to model errors in $\hat{G}_u(s)$, the decoupling condition of the control input u is not fully satisfied by the filters $Q^a(s)$ and $Q^b(s)$, i.e., $R_u(s) \neq 0$. A more accurate model, described in Chapter 4, can reduce the presence of r in the residuals.

Finally, it is observed in residual ε_3 that the influence of sensor noise w on the residuals can be greatly reduced via $Q^b(s)$, which employs the AFDIP algorithm (—).

6.2 Detecting actuator and sensors faults for unsuspended systems

6.2.1 Experimental setup

The OAT contains a lightweight motion stage which can be positioned in all 6 DOF. The stage is levitated via four gravitation compensators in the corners and contains 7 sensors of which 4 sensors measure the z -direction, 2 sensors measure the x -direction and 1 sensor measures the y -direction, see Fig 6.6 (a). The position in the z -direction is measured in the corners of the stage via linear incremental encoder with a resolution of 1 nm. The stage is actuated by Lorenz-actuators of which 13 actuate in the z -direction, 2 actuate in the x -direction and 2 actuate in the y -direction, see

Fig 6.6 (b). The system has a sample frequency of 10 kHz and is closed-loop controlled.

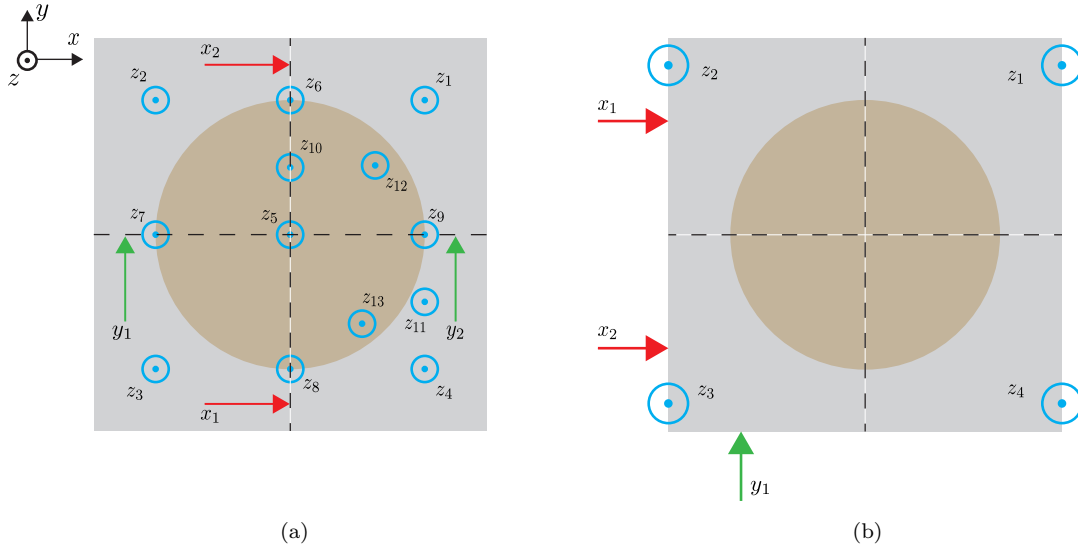


Fig. 6.6: Schematic top view of the OAT. On the left side, the stage of the OAT which is sensed by 2 sensors in the x -direction (—), 1 sensor in the y -direction (—) and 4 sensors in the z -direction (○). on the right side, the stage of the OAT which is actuated by 2 actuators in the x -direction (—), 2 actuators in the y -direction (—) and 13 actuators in the z -direction (○).

For this case-study, the fault diagnosis is limited to the z -direction of the stage, i.e., the detection of 4 actuators and 4 sensor faults. A closed-loop system identification is performed to obtain an FRF. A 20-th order approximate model $\hat{G}_u(s)$ is fitted on the FRF to obtain $\hat{G}_u(s) : [u_1 \ u_2 \ u_3 \ u_4]^T \rightarrow [z_1 \ z_2 \ z_3 \ z_4]^T$, where u_1 to u_4 are the 4 z -actuator in Fig 6.6(a) and z_1 to z_4 are the 4 sensors in Fig 6.6(b). The model $\hat{G}_u(s)$ and the FRF are depicted in Fig 6.7.

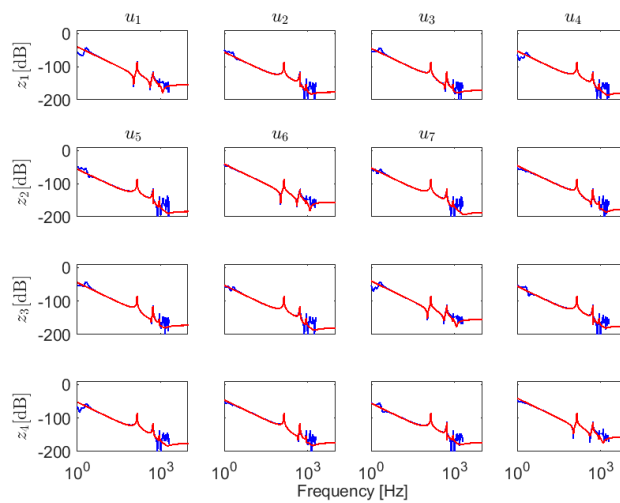


Fig. 6.7: The 20-th order approximate model $\hat{G}_u(s)$ (—) fitted on the measured frequency response function (—) of the overactuated test rig (OAT). The model is limited to the z -direction (height) of the OAT.

For control purposes, the system is again decoupled via the matrices T_u and T_y , such that the modal system is $G_u^{mod} = T_y G_u T_u$. Decentralized controllers are employed to control the 6 DOF and a fourth order setpoint is injected into the rigid loop. The reference has a maximum amplitude of 100 μm .

6.2.2 FDI design

The closed-loop system of the OAT, including the FDI filters $Q(s)$ and the fault injections, is depicted in Fig 6.8. The fault inputs f_1 to f_4 correspond to the actuator faults u_1 to u_4 respectively. The fault inputs f_5 to f_8 correspond to the sensor faults z_1 to z_4 , respectively. For the fault inputs, a step input is injected, i.e., abrupt changes. A step input of 0.1 N is applied to the actuators u_1 to u_4 and a step input of 10 μm is applied to the four sensors z_1 to z_4 . The step inputs are injected consecutively.

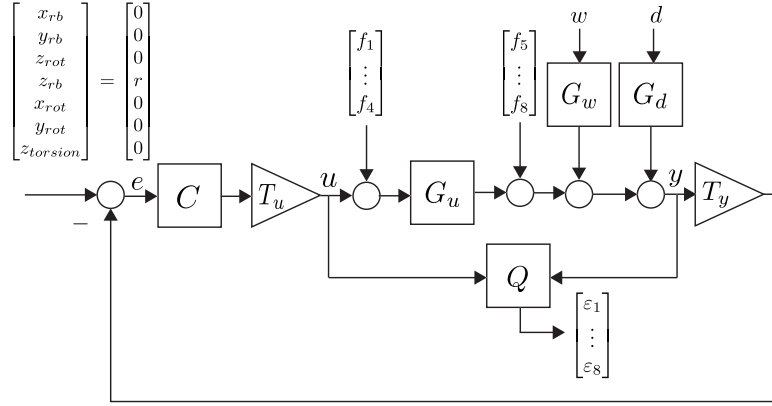


Fig. 6.8: Closed-loop control scheme of the OAT including the employed FDI filters $Q(s)$ and the injected actuator and sensor faults. The residuals ε indicate the presence or absence of fault f .

To detect and localize these 8 faults (4 actuators and 4 sensors faults), a bank of FDI filters $Q(s) \in \mathbb{R}(s)^{8 \times 8}$ is synthesized based on the 20-th order model $\hat{G}_u(s)$. The EFDIP algorithm is employed to synthesize $Q(s)$. The employment of the AFDIP algorithm is neglected, due to the small presence of noise in the setup. The following design parameters are used: $G_u(s) = \hat{G}_u(s)$, $G_d(s) = 0$, $G_w(s) = 0$, **smarg** = -1, **sdeg** = -3, **nullspace** = true, **minimal** = false, **SFDI** = $S^{8 \times 8}$, **HDesign** = h , **tol** = $1e-9$. The minimality option is disabled due to the poor performance of the synthesized filter. Therefore, detectors are hand-pick via the matrix h . In addition, a low-pass filter of $\frac{1}{s+3}$ is employed on the FDI filters to remove any undesired direct-feedthrough terms.

$$S^{8 \times 8} = \begin{bmatrix} 0 & 1 & 1 & 1 & 0 & 1 & 1 & 1 \\ 1 & 0 & 1 & 1 & 1 & 0 & 1 & 1 \\ 0 & 1 & 0 & 1 & 1 & 1 & 0 & 1 \\ 1 & 1 & 1 & 0 & 1 & 1 & 1 & 0 \\ 1 & 1 & 1 & 1 & 0 & 1 & 1 & 1 \\ 1 & 1 & 1 & 1 & 1 & 0 & 1 & 1 \\ 1 & 1 & 1 & 1 & 1 & 1 & 0 & 1 \\ 1 & 1 & 1 & 1 & 1 & 1 & 1 & 0 \end{bmatrix}, h = \begin{bmatrix} 1 & 0^{1 \times 19} \\ 0^{1 \times 3} & 1 & 0^{1 \times 16} \\ 0^{1 \times 4} & 1 & 0^{1 \times 15} \\ 0^{1 \times 6} & 1 & 0^{1 \times 13} \\ 0^{1 \times 9} & 1 & 0^{1 \times 10} \\ 0^{1 \times 11} & 1 & 0^{1 \times 8} \\ 0^{1 \times 15} & 1 & 0^{1 \times 4} \\ 1^{1 \times 18} & 1 & 0^{1 \times 1} \end{bmatrix}. \quad (6.2)$$

The fault-to-residual TFM $R_f(s)$, is depicted in Fig 6.9. Observe that the sensor faults, f_5 to f_8 , are not strong detectable at $\Omega = \{0\}$ in all the residuals. This results from the decoupling of one sensor input.

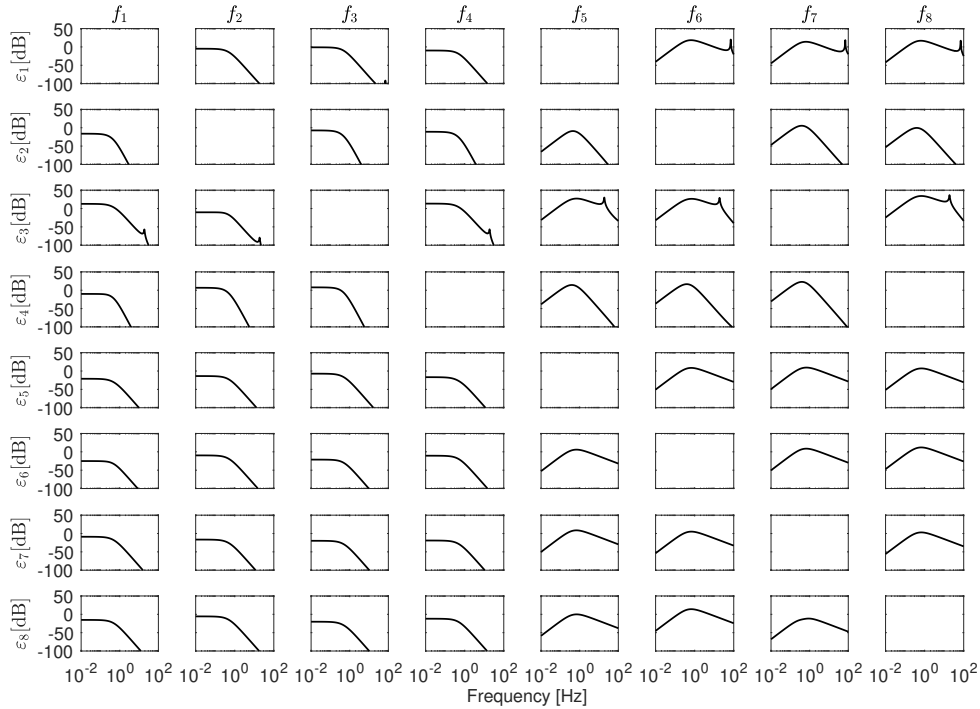


Fig. 6.9: The fault-to-residual TFM $R_f(s)$ synthesized via the EFDISYN algorithm (—). The faults f_1 to f_4 correspond to four actuator faults. The faults f_5 to f_8 correspond to four sensor faults. The synthesis is based on the 20-th order model $\hat{G}_u(s)$ of the overactuated test rig.

6.2.3 Result

The residual signals of the FDI filters $Q(s)$, generated via the EFDIP algorithm, are depicted in Fig 6.10. Note, that $Q(s)$ is only employed experimental.

First, observe that the injected actuator faults f_1 to f_4 , between the time steps 0 to 40 seconds, are visible in all the residuals. The residuals ε_i for $i = \{1, \dots, 4\}$ do not respond to the fault f_j , where $i = j$, since this is enforced via the binary matrix S .

Second, the injected sensor faults f_5 to f_8 , at the time steps 43, 53, 63 and 73 seconds, are difficult to distinguish in the residuals. This can also be concluded from the fault-to-residual response $R_f(s)$ in Fig 6.9, in which the sensor fault inputs have almost an identical magnitude as the actuator inputs at $\Omega = \{0\}$. With the substantial difference between the actuator and sensor fault input, which is $\frac{0.1}{1e-5} = 1e4$, the actuator faults dominate the residual signals.

Third, the presence of the peaks between 40 and 80 seconds, after injecting the sensor faults, are caused by abrupt changes in the actuators forces. Since, the sensor fault introduces a position error in one of the sensors, the controller then corrects the change in height by introducing a step in the actuator forces. Injecting a smaller value for the sensor fault, e.g., with an amplitude of $1 \mu\text{m}$, reduces the change in the actuator forces drastically. However, a low magnitude for the sensor fault magnitude, results in a residual in which the sensor fault is not distinguishable in the residuals. This is due to the presence of the reference signal, which is then more dominant than the sensor fault signal. This presence of the reference in the residuals is caused by model errors present in the approximate model.

Lastly, the isolation of the faults is not fully satisfied, since the residual signals do not correspond with the structure of $R_f(s)$. For example, the sensor fault f_5 , injected at 43 seconds, is present in residual ε_5 , while this fault should be decoupled in fault detector $Q^5(s)$, see Fig 6.9. This is again caused by the model errors present in the approximate model.

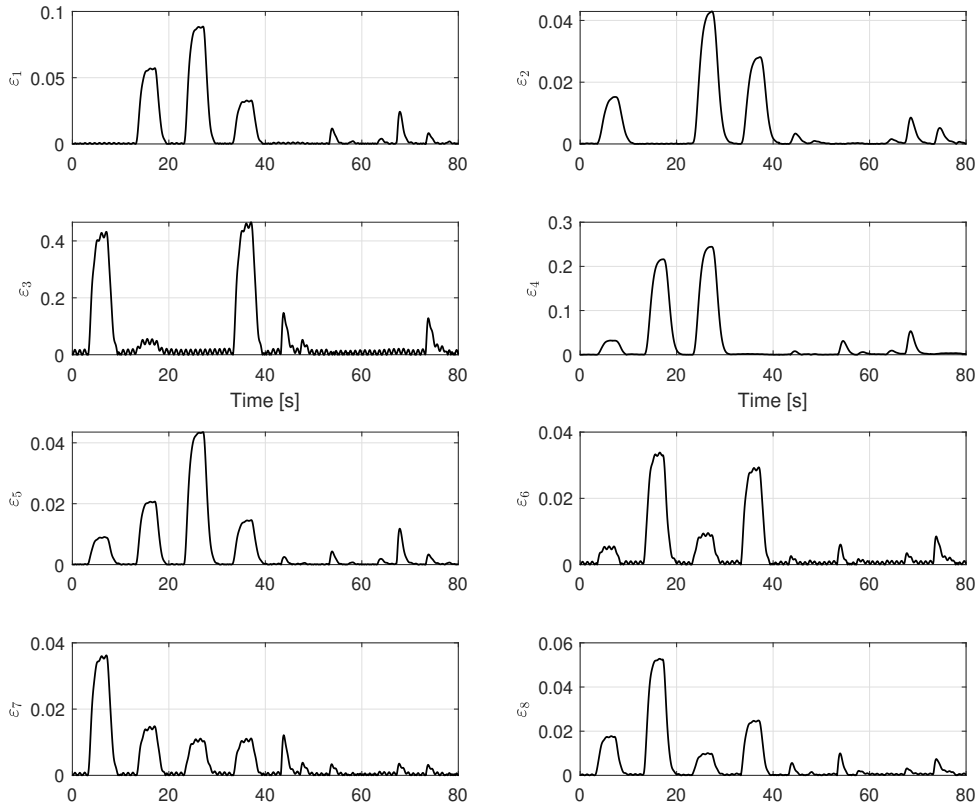


Fig. 6.10: The residual signals of the fault detectors $Q(s)$ employed on the overactuated test rig. The residual signals are processed by taking the absolute value. The four injected actuator faults of 0.1 N are visible in the first 40 seconds. The four injected sensor faults of 10 μm , are less visible in the time range of 40 and 80 seconds, due to the low sensor fault magnitude. Additionally, isolation is not fully satisfied due to the presence of model errors.

6.3 Real-time interference decoupling

6.3.1 Cable slab behaviour

One of the challenges for employing a fault diagnosis system at a submodule level, is the presence of interferences and/or interactions in MIMO systems. In this case-study, the effect of interference in the residuals of the FDI filter $Q(s)$ is investigated. Therefore, a virtual cable slab force f_{cable} is introduced in the OAT, which is defined as a disturbance force.

To simulate cable slab behaviour in the OAT, a virtual cable slab force is generated which is contrary to the position reference and introduced to one of the motors. In this case-study, a force is introduced to actuator z_6 in Fig 6.6(a). In Fig 6.11 a schematic side view is shown of the OAT with the virtual cable slab in (■).

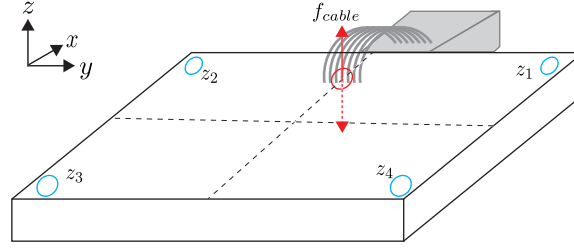


Fig. 6.11: The position of the considered sensors and actuators of the overactuated test rig (\circ). The actuator at position (\circ) simulates the virtual cable slab force (\blacksquare).

6.3.2 FDI design for cable slab detection

Consider the following assumptions:

Assumption 2. *It is assumed that the approximate parametric model $\hat{G}_u(s) : [u_1 \ u_2 \ u_3 \ u_4]^T \rightarrow [z_1 \ z_2 \ z_3 \ z_4]^T$ is available. Therefore, a 14-th order OAT model is used.*

Assumption 3. *It is assumed that the parametric model $G_{cable}(s) : [u_6]^T \rightarrow [z_1 \ z_2 \ z_3 \ z_4]^T$ is available. This model can be obtained via techniques such as the finite element methods (FEM) or via shaker excitation. In this case-study, the model is derived from a 14-th order OAT model.*

Assumption 4. *It is assumed that only the actuators $[u_1 \ u_2 \ u_3 \ u_4]$ can be faulty, i.e., $G_f(s) = \hat{G}_u(s)$.*

Assumption 5. *It is assumed that $G_d(s) = G_{cable}(s)$*

Assumption 6. *It is assumed that $G_w(s) = 0$.*

A bank of filters $Q(s) \in \mathbb{R}(s)^{4 \times 8}$ is synthesized, via the algorithm EFDISYN, to detect the four actuator faults. The design parameters are: $G_u(s) = \hat{G}_u(s)$, $G_d(s) = G_{cable}(s)$, $G_w(s) = 0$, **smarg** = -1, **sdeg** = -3, **nullspace** = true, **minimal** = false, **SFDI** = $S^{4 \times 4}$. The minimality option is disabled due to the poor performance of the synthesized filter.

$$S^{4 \times 4} = \begin{bmatrix} 0 & 1 & 1 & 1 \\ 1 & 0 & 1 & 1 \\ 1 & 1 & 0 & 1 \\ 1 & 1 & 1 & 0 \end{bmatrix}, h = \begin{bmatrix} 1 & 0 & 0 & 0 & 0 & 0 & 0 & 0 \\ 0 & 0 & 1 & 0 & 0 & 0 & 0 & 0 \\ 0 & 0 & 0 & 0 & 1 & 0 & 0 & 0 \\ 0 & 0 & 0 & 0 & 0 & 0 & 1 & 0 \end{bmatrix}$$

A low-pass filter of $\frac{1}{s+3}$ is employed to $Q(s)$ to remove any undesired direct-feedthrough terms. Additionally, a second bank of FDI filters is synthesized to visualize the effect of the cable slab interference. The synthesis has the same design options to generate a bank of FDI filters $Q(s)$, except for one options: $G_d(s) = 0$. The corresponding fault-to-residual TFM $R_f(s) \in \mathbb{R}(s)^{4 \times 4}$ of both filters, are depicted in Fig 6.12. Observe that strong fault detectability is lost in the residuals ε_3 and ε_4 , after decoupling of the cable slab.

The introduced force of the virtual cable slab, i.e., disturbance signal d , has a maximum value of 0.1 N. The fault injection on the actuators u_1 to u_4 are step inputs with an amplitude of 0.1 N and are injected consecutively. The reference of the rigid body has a maximum amplitude of 100 μm .

6.3.3 Result

The residuals of both filters, accumulated from experiments, are shown in Fig 6.13. First, observe that the interference of the virtual cable slab is drastically reduced by the decoupling of G_{cable} in Fig 6.13 (b). However, the cost of this procedure is the loss of the strong detectability property

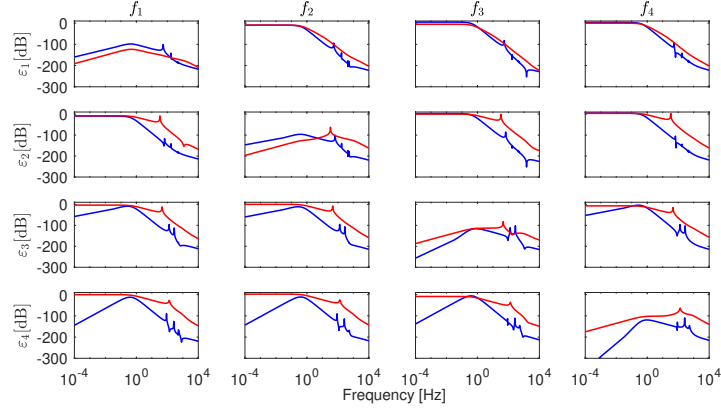


Fig. 6.12: The fault-to-residual TFM $R_f(s)$ (—) of synthesized FDI filters $Q(s)$, including the decoupling of the virtual cable slab interference in the synthesis. The $R_f(s)$ (—) of synthesized FDI filters $Q(s)$, neglecting virtual cable slab interference.

in the filter $Q^3(s)$ and $Q^4(s)$, as the faults fade away in the residuals ε_3 and ε_4 . This can also be observed in Fig 6.12, where $R_f^3(s)$ and $R_f^4(s)$ has zeros present at $\Omega = \{0\}$. Nevertheless, the faults are still visible.

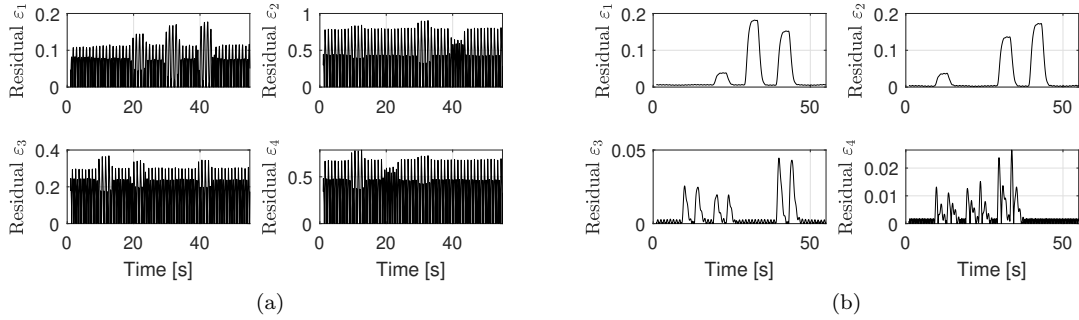


Fig. 6.13: The generated residual signals of the employed FDI filters on the overactuated test rig. The four actuator faults are difficult to distinguish in (a) since cable slab interference is neglected during the synthesis. In the residuals on the right side, the actuator faults are clearly visible, since the cable slab interference is decoupled during the synthesis.

Chapter 7

Conclusions & Recommendations

7.1 Conclusions

To reduce unscheduled production downtime, fault diagnostic systems are essential in MIMO high-tech precision machines. This report investigated the employment of the nullspace-based approach for fault diagnosis, to detect and localize actuator and sensor faults.

The results show that the detection and localization of actuator and sensor faults in high-precision systems are limited. In particular, the detection and localization of abrupt sensor faults is restricted in systems which have poles at the origin, i.e., unsuspended systems. Additionally, the localization of actuator and/or sensor faults is not possible in case of identical dynamics between inputs-outputs in a MIMO system.

Regarding the model requirements for nullspace-based fault diagnosis, it is important to have an accurate plant model in the lower frequency region. In case of modelling errors in the approximated models, the residual of the fault detector contains remnants of other signals than the fault input f . Experimental results show the presence of undesired reference r , due to modelling errors in the plant model, which makes it difficult to distinguish the faults.

Experimental results also demonstrated that employing fault diagnosis system on a submodule level is feasible. By including the interference from another submodule during the synthesis of a fault detector, it is shown that the effect of the interference signal was greatly reduced.

7.2 Recommendations

As a result of model mismatch, the residual signals in the experiments still had remnants of the reference. To improve the decoupling of the control input u , a more accurate model of the plant is required. This would improve the visualization of the faults.

The limitation of the nullspace-based fault diagnosis has been analytically investigated for simple mass and mass-spring systems. However, the limitation does not cover systems containing zeros, e.g., mass-spring-damper systems or systems including flexible modes. This introduces new mathematical challenges to prove whether actuator and/or sensor faults are strong fault detectable or isolatable.

Lastly, it is demonstrated that interferences between submodules can be greatly reduced on submodule level. However, in case of interaction between submodules, a different design strategy for the fault detection filter might be required. For the synthesis of an effective fault diagnosis system, interaction terms have to be included in the model [14]. These interaction models are often of high order. Including these interaction models into the synthesis of the fault diagnosis system, drastically increases the order of the fault detection filter, which is not desirable.

Bibliography

- [1] X. Chen, S. Wang, B. Qiao and Q. Chen, “Basic research on machinery fault diagnostics: Past, present, and future trends,” *Frontiers of Mechanical Engineering*, vol. 13, no. 2, pp. 264–291, 2018.
- [2] K. Classens, W. P. M. H. Heemels and T. Oomen, “Digital twins in mechatronics: From model-based control to predictive maintenance,” in *1st International Conference on Digital Twins and Parallel Intelligence (DTPI)*, Beijing, China, 2021, pp. 336–339.
- [3] I. V. de Bessa, R. M. Palhares, M. F. S. V. D’Angelo and J. E. Chaves Filho, “Data-driven fault detection and isolation scheme for a wind turbine benchmark,” *Renewable Energy*, vol. 87, pp. 634–645, 2016.
- [4] M. Li, D. Yu, Z. Chen, K. Xiahou, T. Ji and Q. H. Wu, “A data-driven residual-based method for fault diagnosis and isolation in wind turbines,” *IEEE Transactions on Sustainable Energy*, vol. 10, no. 2, pp. 895–904, 2019.
- [5] D. Jung and C. Sundstrom, “A combined data-driven and model-based residual selection algorithm for fault detection and isolation,” *IEEE Transactions on Control Systems Technology*, vol. 27, no. 2, pp. 616–630, 2019.
- [6] G. I. Gheorghe, Ed., *Proceedings of the International Conference of Mechatronics and Cyber-Mix Mechatronics*, vol. 48, Cham: Springer International Publishing, 2019.
- [7] S. X. Ding, *Model-based fault diagnosis techniques: design schemes, algorithms and tools* (Advances in industrial control), 2nd ed. New York: Springer, 2013.
- [8] A. Varga, *Solving Fault Diagnosis Problems*. Cham: Springer International Publishing, 2017, vol. 84.
- [9] S. Hecker, A. Varga and G. Looye, “A desktop environment for assessment of fault diagnosis based fault tolerant flight control laws,” in *IEEE International Conference on Computer-Aided Control Systems*, San Antonio, TX, USA, 2008, pp. 195–200.
- [10] D. Ossmann and F. L. J. van der Linden, “Advanced sensor fault detection and isolation for electro-mechanical flight actuators,” in *NASA/ESA Conference on Adaptive Hardware and Systems (AHS)*, Montreal, QC, 2015, pp. 1–8.
- [11] T. Oomen and M. Steinbuch, “Model-based control for high-tech mechatronic systems,” in *Mechatronics and Robotics*, M. Indri and R. Oboe, Eds., 1st ed. Boca Raton, 2020, pp. 51–80.
- [12] T. Oomen, R. van Herpen, S. Quist, M. van de Wal, O. Bosgra and M. Steinbuch, “Connecting system identification and robust control for next-generation motion control of a wafer stage,” *IEEE Transactions on Control Systems Technology*, vol. 22, no. 1, pp. 102–118, 2014.
- [13] T. C. J.P.M.B. Vermeulen, *Challenges in next-generation substrate positioning*, 2010.
- [14] K. Classens, W. P. M. H. Heemels and T. Oomen, “Closed-loop aspects in MIMO fault diagnosis with application to precision mechatronics,” in *American Control Conference (ACC)*, New Orleans, LA, USA, 2021, pp. 1756–1761.
- [15] S. Skogestad and I. Postlethwaite, *Multivariable feedback control: analysis and design*, 2. ed., repr. Chichester: Wiley, 2010, 574 pp.
- [16] E. Frisk and M. Nyberg, “A minimal polynomial basis solution to residual generation for fault diagnosis in linear systems,” *Automatica*, 37th ser., pp. 1417–1424, 2001.

- [17] A. Varga, "On computing nullspace bases, a fault detection perspective," *IFAC Proceedings Volumes*, vol. 41, no. 2, pp. 6295–6300, 2008.
- [18] A. Varga, "On computing least order fault detectors using rational nullspace bases," *IFAC Proceedings Volumes*, vol. 36, no. 5, pp. 227–232, 2003.
- [19] T. T. Beelen, "New algorithms for computing the kronecker structure of a pencil with applications to systems and control theory," Publisher: Technische Universiteit Eindhoven, Ph.D. dissertation, Eindhoven University of Technology, 1987.
- [20] P. Dooren, G. Verghese and T. Kailath, "Properties of the system matrix of a generalized state-space system," in *IEEE Conference on Decision and Control including the 17th Symposium on Adaptive Processes*, San Diego, CA, USA, 1978, pp. 173–175.
- [21] A. Varga, "Reliable algorithms for computing minimal dynamic covers," in *International Conference on Decision and Control*, Maui, Hawaii, USA, 2003, pp. 1873–1878.
- [22] A. Varga, "Computation of irreducible generalized state-space realizations," *Kybernetika*, vol. no. 26, pp. 89–106, 1990.
- [23] A. Varga, "On recursive computation of coprime factorizations of rational matrices," *Linear Algebra and its Applications*, vol. 623, pp. 478–502, 2021.
- [24] A. Varga, "Descriptor system techniques in solving $H_{2/\infty}$ optimal fault detection and isolation problems," in *Control and Optimization with Differential-Algebraic Constraints*, Philadelphia, PA: Society for Industrial and Applied Mathematics, 2012, pp. 105–126.
- [25] K. Zhou, J. C. Doyle and K. Glover, *Robust and optimal control*. Upper Saddle River: Prentice Hall, 1996.
- [26] N. Liu and K. Zhou, "Optimal robust fault detection for linear discrete time systems," *Journal of Control Science and Engineering*, vol. 2008, pp. 1–16, 2008.
- [27] A. Varga, "General computational approach for optimal fault detection," *IFAC Proceedings Volumes*, vol. 42, no. 8, pp. 107–112, 2009.
- [28] K. Glover and A. Varga, "On solving non-standard $H_-/H_{2/\infty}$ fault detection problems," in *Conference on Decision and Control and European Control Conference*, Orlando, FL, USA, 2011, pp. 891–896.
- [29] C. Oara and A. Varga, "Computation of general inner-outer and spectral factorizations," *IEEE Transactions on Automatic Control*, vol. 45, no. 12, pp. 2307–2325, 2000.
- [30] R. van Herpen, T. Oomen and M. Steinbuch, "Optimally conditioned instrumental variable approach for frequency-domain system identification," *Automatica*, vol. 50, no. 9, pp. 2281–2293, 2014.
- [31] R. M. W. Sanders, "Multi-input feedforward design for vibration reduction in motion systems," Master, Eindhoven University of Technology, Eindhoven, 2005, 71 pp.
- [32] P. Lambrechts, M. Boerlage and M. Steinbuch, "Trajectory planning and feedforward design for electromechanical motion systems," *Control Engineering Practice*, vol. 13, no. 2, pp. 145–157, 2005.
- [33] R. Pintelon and J. Schoukens, *System identification: a frequency domain approach*, 2nd ed. Hoboken, N.J: John Wiley & Sons Inc, 2012, 743 pp.
- [34] E. Evers, "Identification and active thermomechanical control in precision mechatronics," Ph.D. dissertation, Eindhoven University of Technology, Eindhoven, 2021.
- [35] A. Varga, "A fault detection toolbox for MATLAB," Munich, Germany, 2006, pp. 3013–3018.

Appendix A

Example of the loss of strong fault detectability for sensor faults in unsuspended systems

Consider the following system

$$G_u(s) = \begin{bmatrix} \frac{1}{s^2} & 0 \\ 0 & \frac{1}{s^2} \end{bmatrix}, G_d(s) = 0, G_f(s) = \begin{bmatrix} \frac{1}{s^2} & 0 & 1 & 0 \\ 0 & \frac{1}{s^2} & 0 & 1 \end{bmatrix}, \quad (\text{A.1})$$

where $G_u(s)$ represents an unsuspended system. Then $G(s)$ is

$$G(s) = \begin{bmatrix} G_u(s) \\ I_2 \end{bmatrix} = \begin{bmatrix} \frac{1}{s^2} & 0 \\ 0 & \frac{1}{s^2} \\ 1 & 0 \\ 0 & 1 \end{bmatrix}. \quad (\text{A.2})$$

The following stable and proper filter $Q(s)$ can be formed to decouple $G(s)$, i.e., $Q(s)G(s) = 0$

$$Q(s) = \begin{bmatrix} \frac{s^2}{(s+1)(s+2)} & 0 & \frac{-1}{(s+1)(s+2)} & 0 \\ 0 & \frac{s^2}{(s+1)(s+2)} & 0 & \frac{-1}{(s+1)(s+2)} \end{bmatrix}, \quad (\text{A.3})$$

The resulting fault-to-residual response $R_f(s)$ is then

$$R_f(s) = Q(s) \begin{bmatrix} G_f(s) \\ 0 \end{bmatrix} = \begin{bmatrix} \frac{1}{(s+1)(s+2)} & 0 & \frac{s^2}{(s+1)(s+2)} & 0 \\ 0 & \frac{1}{(s+1)(s+2)} & 0 & \frac{s^2}{(s+1)(s+2)} \end{bmatrix}. \quad (\text{A.4})$$

Both $R_{f_3}^1(s)$ and $R_{f_4}^2(s)$ have zeros in Ω due to the s^2 numerator. Hence, the sensor faults are not strong fault detectable by $Q(s)$, i.e., the $Q(s)$ is not Ω -admissible.

Appendix B

Example of limitation of fault isolation in high-tech precision systems

Consider the MIMO plant $G_u(\lambda) \in \mathbb{R}(\lambda)^{3 \times 3}$, $G_d(\lambda) = 0$ and $G_w(\lambda) = 0$. The MIMO plant is obtained from a high-tech system and can be written as

$$G_u(\lambda) = N(\lambda)/d(\lambda), \quad (\text{B.1})$$

where $N(\lambda)$ is the numerator TFM and $d(\lambda)$ is the common denominator. Assume that both actuator and sensor faults have to be detected and isolated. Hence, the fault-to-residual response is equal to

$$R_f(\lambda) = G_f(\lambda) = [G_u(\lambda) \quad I_3] = \frac{1}{d(\lambda)} [N(\lambda) \quad d(\lambda)] \quad (\text{B.2})$$

For the binary matrix S , the following structure is chosen

$$S = [0 \quad 1 \quad 1 \quad 1 \quad 1 \quad 0] \quad (\text{B.3})$$

Hence, the first and last column of R_f are considered as disturbances and are decoupled via the nullspace method, i.e., $\hat{G}_d = [R_1(\lambda) \quad R_6(\lambda)]$. A factor $\bar{Q}_y(\lambda)$ is computed such that

$$\bar{Q}_y(\lambda)R_f(\lambda) = \bar{R}_f(\lambda), \quad (\text{B.4})$$

where $\bar{R}_f(\lambda)$ has the same structure as S . In other words,

$$\underbrace{\begin{bmatrix} \bar{Q}_{y_1}(\lambda) \\ \vdots \\ \bar{Q}_{y_3}(\lambda) \end{bmatrix}}_{\bar{Q}_y(\lambda)} \frac{1}{d(\lambda)} \underbrace{\begin{bmatrix} N_{11}(\lambda) & \cdots & N_{13}(\lambda) & d(\lambda) & \cdots & 0 \\ \vdots & \ddots & \vdots & \vdots & \ddots & \vdots \\ N_{31}(\lambda) & \cdots & N_{33}(\lambda) & 0 & \cdots & d(\lambda) \end{bmatrix}}_{R_f(\lambda)} = \underbrace{[\bar{R}_1(\lambda) \quad \cdots \quad \bar{R}_6(\lambda)]}_{\bar{R}_f(\lambda)}. \quad (\text{B.5})$$

Hence, this can be formulated to the following equalities that have to be satisfied:

$$\begin{aligned} \bar{Q}_{y_1}(\lambda)N_{11}(\lambda) + \bar{Q}_{y_2}(\lambda)N_{21}(\lambda) + \bar{Q}_{y_3}(\lambda)N_{31}(\lambda) &= 0 \\ \bar{Q}_{y_1}(\lambda)N_{12}(\lambda) + \bar{Q}_{y_2}(\lambda)N_{22}(\lambda) + \bar{Q}_{y_3}(\lambda)N_{32}(\lambda) &\neq 0 \\ \bar{Q}_{y_1}(\lambda)N_{13}(\lambda) + \bar{Q}_{y_2}(\lambda)N_{23}(\lambda) + \bar{Q}_{y_3}(\lambda)N_{33}(\lambda) &\neq 0 \\ \bar{Q}_{y_1}(\lambda)d(\lambda) &\neq 0 \\ \bar{Q}_{y_2}(\lambda)d(\lambda) &\neq 0 \\ \bar{Q}_{y_3}(\lambda)d(\lambda) &= 0. \end{aligned}$$

Using the fact that $\bar{Q}_{y_1}(\lambda) \neq 0$, $\bar{Q}_{y_2}(\lambda) \neq 0$, $\bar{Q}_{y_3}(\lambda) = 0$ and $\bar{Q}_{y_1}(\lambda) = -\bar{Q}_{y_2}(\lambda)N_{21}(\lambda)N_{11}(\lambda)^{-1}$, the equations can be further simplified to:

$$[-\bar{Q}_{y_2}(\lambda)N_{21}(\lambda)N_{11}(\lambda)^{-1} \quad \bar{Q}_{y_2}(\lambda)] = \begin{bmatrix} N_{11}(\lambda) \\ N_{21}(\lambda) \end{bmatrix} = [0] \quad (\text{B.6})$$

and

$$[-\bar{Q}_{y_2}(\lambda)N_{21}(\lambda)N_{11}(\lambda)^{-1} \quad \bar{Q}_{y_2}(\lambda)] = \begin{bmatrix} N_{12}(\lambda) & N_{13}(\lambda) \\ N_{22}(\lambda) & N_{23}(\lambda) \end{bmatrix} \neq [0 \quad 0] \quad (\text{B.7})$$

Factoring out $\bar{Q}_{y_2}(\lambda)$ gives

$$\bar{Q}_{y_2}(\lambda) [-N_{21}(\lambda)N_{11}(\lambda)^{-1} \quad I] = \begin{bmatrix} N_{11}(\lambda) \\ N_{21}(\lambda) \end{bmatrix} = [0], \quad (\text{B.8})$$

and

$$\bar{Q}_{y_2}(\lambda) [-N_{21}(\lambda)N_{11}(\lambda)^{-1} \quad I] = \begin{bmatrix} N_{12}(\lambda) & N_{13}(\lambda) \\ N_{22}(\lambda) & N_{23}(\lambda) \end{bmatrix} \neq [0 \quad 0]. \quad (\text{B.9})$$

Note that (B.8) is satisfied with any value for $\bar{Q}_{y_2}(\lambda)$. Hence, $\bar{Q}_{y_2}(\lambda)$ can be any value except 0, to satisfy (B.9). A filter $\bar{Q}_y(\lambda)$ exists iff there does not exist a α for which

$$\begin{bmatrix} N_{12}(\lambda) & N_{13}(\lambda) \\ N_{22}(\lambda) & N_{23}(\lambda) \end{bmatrix} = \alpha \begin{bmatrix} N_{11}(\lambda) \\ N_{21}(\lambda) \end{bmatrix}, \quad (\text{B.10})$$

i.e., $\begin{bmatrix} N_{11}(\lambda) \\ N_{21}(\lambda) \end{bmatrix}$ is linear independent of $\begin{bmatrix} N_{12}(\lambda) & N_{13}(\lambda) \\ N_{22}(\lambda) & N_{23}(\lambda) \end{bmatrix}$.

Appendix C

Example of losing strong fault detection when employing minimality

Consider the following system for an unsuspended SIMO plant:

$$G_u(s) = \begin{bmatrix} \frac{1}{s^2} \\ \frac{1}{s^2} \end{bmatrix}, G_d(s) = 0, G_w(s) = 0,$$

where both actuator and sensor faults have to be detected, i.e., $G_f(s) = [G_u(s) \ I_2]$. Then the left nullspace basis vectors has to be computed such that $Q(s)G(s) = 0$, where

$$G(s) = \begin{bmatrix} \frac{1}{s^2} \\ \frac{1}{s^2} \\ 1 \end{bmatrix}$$

The following proper and stable left nullspace basis vectors

$$Q(s) = \begin{bmatrix} \frac{s^2}{(s+1)(s+1)} & \frac{s^2}{(s+1)(s+1)} & \frac{-2}{(s+1)(s+1)} \\ 1 & -1 & 0 \end{bmatrix},$$

achieves $Q(s)G(s) = 0$. Hence, $Q(s)$ contains two left nullspace basis vectors. The corresponding fault-to-residual TFM is

$$R_f(s) = Q(s) \begin{bmatrix} G_f(s) \\ 0 \end{bmatrix} = \begin{bmatrix} \frac{2}{(s+1)(s+1)} & \frac{s^2}{(s+1)(s+1)} & \frac{s^2}{(s+1)(s+1)} \\ 0 & 1 & -1 \end{bmatrix}.$$

Now observe that the actuator fault (first column) is strong detectable at $\Omega = \{0\}$ in the first row of $R_f(s)$ but not in the second row of $R_f(s)$. Additionally, the sensors faults (second and third column) are strong detectable in the second row of $R_f(s)$ but not in the first row of $R_f(s)$. Nevertheless, by using both vectors, both actuator and sensor faults are strong detectable.

However, when employing the minimality options, the following stable left nullspace vector is created

$$Q(s) = \begin{bmatrix} \frac{-s^2}{(s+1)(s+1)} & \frac{-s^2}{(s+1)(s+1)} & \frac{2}{(s+1)(s+1)} \end{bmatrix},$$

which satisfies $Q(s)G(s) = 0$. The corresponding fault-to-residual TFM is

$$R_f(s) = Q(s) \begin{bmatrix} G_f(s) \\ 0 \end{bmatrix} = \begin{bmatrix} \frac{-2}{(s+1)(s+1)} & \frac{-s^2}{(s+1)(s+1)} & \frac{-s^2}{(s+1)(s+1)} \end{bmatrix}.$$

Now observe that only the actuator fault (column 1) is strong fault detectable at $\Omega = \{0\}$. Hence, sensor faults are no longer strong fault detectable by $Q(s)$.

Appendix D

Closed-loop transfer functions for nullspace-based fault diagnosis

A closed-loop configuration of the nullspace-based fault detection and isolation is depicted in Fig. D.1. The detection filter $Q := [Q_y \ Q_u]$ is coloured in gray. The detection filter outputs a residual ε which indicates the presence of the fault f and is insensitive to the disturbance w , reference r and disturbance w .

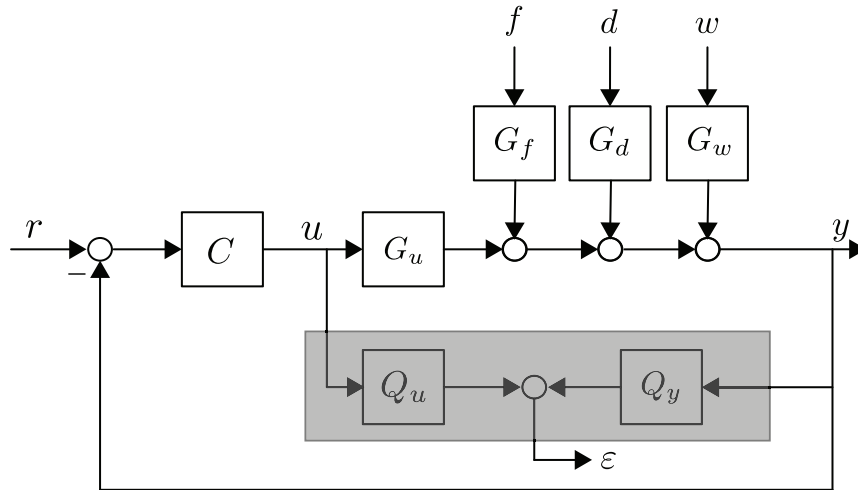


Fig. D.1: Closed-loop configuration with the nullspace-based FDI filter highlighted in (■).

The control input u is formulated as

$$u = CSr - CSG_f f - CSG_d d - CSG_w w \quad (\text{D.1})$$

where $S = (I + G_u C)^{-1}$ is the sensitivity function, G_u is the nominal model of the plant, C is the controller, G_f is the TFM of the fault input f , G_d is the TFM of the disturbance input d and G_w is the TFM of the noise input w . The residual ε is equal to

$$\varepsilon = Q_u u + Q_y y, \quad (\text{D.2})$$

where the open-loop output y can be defined as

$$y = G_u u + G_f f + G_d d + G_w w. \quad (\text{D.3})$$

Substituting (D.3) into (D.2), results in

$$\varepsilon = Q_u u + Q_y (G_u u + G_f f + G_d d + G_w w). \quad (\text{D.4})$$

Assume that via system identification, a model $\hat{G}_u(s)$ and $\hat{G}_d(s)$ are obtained, which are an approximation of the real plant G_u and disturbance G_d , respectively. To decouple the control input u and disturbance d from the residual ε , the nullspace-based fault diagnosis method in [8], synthesizes a filter $Q(s)$ such that

$$\begin{bmatrix} Q_y(s) & Q_u(s) \end{bmatrix} \begin{bmatrix} \hat{G}_u(s) & \hat{G}_d(s) \\ I_{mu} & 0 \end{bmatrix} = 0, \quad (\text{D.5})$$

where mu is the number of control inputs. Then, $Q_u(s)$ can be written as

$$Q_u(s) = -Q_y(s)\hat{G}_u(s). \quad (\text{D.6})$$

Now substituting $Q_u(s)$ in (D.4) with (D.6) gives

$$\varepsilon = -Q_y(s)\hat{G}_u(s)u + Q_y(s)(G_u u + G_f f + G_d d + G_w w), \quad (\text{D.7})$$

which can be rewritten to

$$\varepsilon = Q_y(s)(G_u - \hat{G}_u(s))u + Q_y(s)(G_f f + G_d d + G_w w). \quad (\text{D.8})$$

Then by substituting (D.1) into (D.8), results in

$$\varepsilon = \underbrace{Q_y(G_u - \hat{G}_u(s))(CSr - CSG_f f - CSG_d d - CSG_w w)}_{\text{closed-loop part}} + \underbrace{Q_y(s)(G_f f + G_d d + G_w w)}_{\text{open-loop part}}. \quad (\text{D.9})$$

Notice, that the transfer function can be divided into a closed-loop part and an open-loop part. In case that no model errors are present in $\hat{G}_u(s)$, i.e., $\hat{G}_u(s) = G_u$, the closed-loop part is equal to zero.

To derive the transfer functions $T_{\varepsilon r}$, the other inputs are set to zero, i.e., $f = 0, d = 0, w = 0$. Then the transfer function $T_{\varepsilon r}$ is equal to

$$T_{\varepsilon r} = \frac{\varepsilon}{r} = Q_y(s)(G_u - \hat{G}_u(s))CS. \quad (\text{D.10})$$

For the derivation of the transfer functions $T_{\varepsilon d}$, $T_{\varepsilon w}$ and $T_{\varepsilon f}$, the approach is used. Hence, the transfer functions are

$$T_{\varepsilon f} = \frac{\varepsilon}{f} = Q_y(G_u - \hat{G}_u)(-CSG_f) + Q_y G_f, \quad (\text{D.11})$$

$$T_{\varepsilon d} = \frac{\varepsilon}{d} = Q_y(G_u - \hat{G}_u)(-CSG_d) + Q_y G_d, \quad (\text{D.12})$$

$$T_{\varepsilon w} = \frac{\varepsilon}{w} = Q_y(G_u - \hat{G}_u)(-CSG_w) + Q_y G_w. \quad (\text{D.13})$$

Appendix E

Example loss of fault isolability due to row and column independency

Consider the following system

$$G_u(s) = \begin{bmatrix} \frac{1}{s^2} & \frac{2}{s^2} \\ \frac{2}{s^2} & \frac{1}{s^2} \end{bmatrix}, G(s) = \begin{bmatrix} \frac{1}{s^2} & \frac{2}{s^2} \\ \frac{2}{s^2} & \frac{1}{s^2} \\ 1 & 0 \\ 0 & 1 \end{bmatrix}, G_f(s) = \begin{bmatrix} \frac{1}{s^2} & \frac{2}{s^2} & 1 & 0 \\ \frac{2}{s^2} & \frac{1}{s^2} & 0 & 1 \end{bmatrix}. \quad (\text{E.1})$$

Observe that the row and columns of $G_u(\lambda)$ are independent. Then a stable and proper fault detector $Q(s)$ has to be computed such that

$$Q(s)G(s) = 0. \quad (\text{E.2})$$

Recall that the fault detector can be presented as $Q(s) = [Q_y(s) \quad Q_u(s)]$. Hence,

$$[Q_{y_1} \quad Q_{y_2} \quad Q_{u_1} \quad Q_{u_2}] \begin{bmatrix} \frac{1}{s^2} & \frac{2}{s^2} \\ \frac{2}{s^2} & \frac{1}{s^2} \\ 1 & 0 \\ 0 & 1 \end{bmatrix} = 0. \quad (\text{E.3})$$

However, since $G_u(s)$ has linear independent rows and columns, there does not exist a solution for $Q(s)$, where $Q_y(s)$ only contains constant values. Hence, $Q_y(s)$ contains zeros at frequency $\Omega = \{0\}$ to cancel the unstable poles at Ω of $G(s)$. This causes the fault-to-residual response $R_f(s)$ to contain zeros in Ω , i.e., faults are not strong fault detectable. The calculation of $R_f(s)$ are left open for the reader.